CANCER

Endogenous DOPA inhibits melanoma through suppression of CHRM1 signaling

Miriam Doepner[1], Inyoung Lee[1], Christopher A. Natale[1], Roderick Brathwaite[1], Swati Venkat[2], Sung Hoon Kim[3], Yiliang Wei[4], Christopher R. Vakoc[4], Brian C. Capell[1], John A. Katzenellenbogen[3], Benita S. Katzenellenbogen[5], Michael E. Feigin[2], Todd W. Ridky[1]*

Melanoma risk is 30 times higher in people with lightly pigmented skin versus darkly pigmented skin. Using primary human melanocytes representing the full human skin pigment continuum and preclinical melanoma models, we show that cell-intrinsic differences between dark and light melanocytes regulate melanocyte proliferative capacity and susceptibility to malignant transformation, independent of melanin and ultraviolet exposure. These differences result from dihydroxyphenylalanine (DOPA), a melanin precursor synthesized at higher levels in melanocytes from darkly pigmented skin. We used both high-throughput pharmacologic and genetic in vivo CRISPR screens to determine that DOPA limits melanocyte and melanoma cell proliferation by inhibiting the muscarinic acetylcholine receptor M_1 (CHRM1) signaling. Pharmacologic CHRM1 antagonism in melanoma leads to depletion of c-Myc and FOXM1, both of which are proliferation drivers associated with aggressive melanoma. In preclinical mouse melanoma models, pharmacologic inhibition of CHRM1 or FOXM1 inhibited tumor growth. CHRM1 and FOXM1 may be new therapeutic targets for melanoma.

INTRODUCTION

Melanoma is the most lethal form of skin cancer on a per case basis. Despite advances in modern immune and targeted therapies, most patients with metastatic melanoma succumb to their disease and additional treatment approaches are needed (*1*, *2*). Clues to therapeutic approaches may lie in understanding the mechanisms by which melanoma differentially affects different populations of people. Here, we consider why the lifetime risk for cutaneous melanoma is substantially higher for people with lightly pigmented skin compared to those with darkly pigmented skin, even when they live in the same geographic region and are thereby exposed to similar amounts of ultraviolet radiation (UVR) (*3*).

Melanoma develops from melanocytes (MCs), which normally reside in the basal layer of skin and hair follicles where they produce melanin pigment, the primary determinant of skin and hair color. Melanogenesis is a complex, multistep process that begins with the nonessential amino acid L-tyrosine and results in the production of mostly insoluble eumelanin (brown-black) or pheomelanin (red-yellow) polymers (*4*–*6*). Variation in the eumelanin content is a major determinant of the natural diversity in human skin pigmentation, as pheomelanin remains constant across populations (*7*). These baseline pigmentary differences result from numerous single-nucleotide polymorphisms (SNPs) in at least 200 genes involved in melanin synthesis (*8*). Eumelanin acts as a physical photoprotective filter against DNA damaging solar UVR and thereby protects skin cells from deleterious mutations that may lead to malignant transformation (*9*). While melanin's UVR shielding effect undoubtedly accounts for some of the differences in lifetime melanoma risk across the diverse human pigment continuum, highly pigmented skin provides a sun protective factor (SPF) of only 2 to 3 versus lightly pigmented skin, which seems insufficient to completely explain the large 30-fold difference in melanoma incidence between people with lightly pigmented versus darkly pigmented skin (*10*, *11*). Furthermore, a UVR shielding effect does not fully explain decades of epidemiologic data, suggesting that there are UV-independent determinants of melanoma risk that also correlate with skin pigment type. Melanomas arising in completely sun-protected areas, such as anorectal melanoma, are up to 13 times more common in people with lightly versus highly pigmented skin (*12*, *13*). There are also intriguing observations involving skin cancer in people from Africa with albinism. While many cases of human albinism result from mutations in tyrosinase (Tyr), the rate-limiting enzyme in melanin synthesis, the most prevalent type of albinism in Africa is caused by a mutation in OCA2, which is associated with maintenance of some Tyr activity (*14*, *15*). While OCA2-affected individuals have epidermal MCs, they make very little melanin and therefore have white or extremely lightly pigmented skin and hair. They exhibit photosensitivity and an expected elevated incidence of keratinocyte-derived cancers, including basal cell and squamous cell carcinomas. However, they appear highly resistant to melanoma, suggesting that while their MCs are visibly light, they may be functionally "dark" with regard to melanoma, and thereby similar to those with darkly pigmented skin in their population group with shared African ancestry (*16*, *17*). The mechanism(s) underlying these apparent UV-independent determinants of melanoma susceptibility were previously unknown, but this clinical observation served as some of the rationale for us to begin exploring the possibility that the increased melanoma susceptibility in lightly pigmented skin results from factors beyond physical UV shielding from melanin.

Here, we demonstrate that endogenously produced dihydroxyphenylalanine (DOPA), a melanin synthesis intermediate, drives cellular differentiation in primary human MCs, which is associated with slower proliferation and resistance to the oncogenic effects of the major human melanoma oncoprotein BRAF(V600E). We show

[1]Department of Dermatology, Perelman School of Medicine, University of Pennsylvania, Philadelphia, PA, USA. [2]Department of Pharmacology and Therapeutics, Roswell Park Comprehensive Cancer Center, Buffalo, NY, USA. [3]Department of Chemistry and Cancer Center, University of Illinois at Urbana-Champaign, Urbana, IL, USA. [4]Cold Spring Harbor Laboratory, Cold Spring Harbor, NY 11724, USA. [5]Departments of Molecular and Integrative Physiology and Cancer Center, University of Illinois at Urbana-Champaign, Urbana, IL, USA.
*Corresponding author. Email: ridky@pennmedicine.upenn.edu

that these DOPA effects result from antagonism of the muscarinic acetylcholine receptor M_1 (CHRM1), a G protein–coupled receptor (GPCR) on MCs and melanoma cells. In preclinical in vivo melanoma models, pharmacologic CHRM1 antagonism inhibited melanoma growth. CHRM1 inhibition depleted FOXM1, a transcription factor and cell cycle regulator associated with more aggressive cancer, and a new class of FOXM1-specific antagonists also significantly inhibited melanoma growth in vivo and extended overall survival. Together, these data suggest that CHRM1 and FOXM1 may represent previously unidentified druggable targets for melanoma and emphasize that differences in melanoma risk across the human skin pigment continuum are more complex than can be explained simply by a physical UV shielding effect from melanin.

RESULTS

Darkly pigmented MCs are less tumorigenic than light pigmented MCs

Primary human MCs were isolated from neonatal foreskin and grown under standard cell culture conditions without UVR. MCs were used at a low passage number, moderate confluence, and without cryopreservation. We defined lightly pigmented MC (LMC) and darkly pigmented MC (DMC) populations based on their relative melanin content. For this study, LMCs contained at least 10 times less melanin than DMC. Under these cell culture conditions, LMCs proliferated two to three times faster than DMCs (Fig. 1A). MC proliferative capacity is classically inversely correlated with MC cellular differentiation state (*18*–*22*), which is primarily regulated by the activation of G_s-coupled GPCRs (*23*–*26*). G_s signaling stimulates production of cyclic adenosine monophosphate (cAMP) via adenylate cyclase. In MCs, cAMP activates protein kinase A (PKA), which phosphorylates and activates the cAMP response element–binding protein (CREB), to promote downstream synthesis of proteins involved in melanin production, such as Tyr (*27*). We examined whether the expression of proteins within this classic GPCR pathway differed between LMCs and DMCs. DMCs contained more phosphorylated CREB and Tyr than LMCs (fig. S1A), suggesting that DMCs are more fully advanced along a cellular differentiation continuum that parallels the natural range of human skin pigment diversity (*22*, *27*). Consistent with this idea, DMCs generally expressed less of the stem cell marker and oncoprotein c-Myc (Fig. 1B and fig. S1, A and B). We did note some heterogeneity among the cultures, which we expected as these studies used primary MCs from several different people and reflect natural human genetic diversity.

We hypothesized that these baseline differences in relative cellular differentiation state and proliferative capacity between DMCs and LMCs contribute to overall differential melanoma susceptibility. To test this in vivo, we used a genetically defined orthotopic human melanoma (heMel) model (*28*, *29*). Primary LMCs and DMCs were engineered using lentiviruses to express mutant oncoproteins associated with spontaneous human melanoma including $BRAF^{V600E}$, dominant-negative $p53^{R248W}$, active $CDK4^{R24C}$, and hTERT (*29*). Expression of the transduced oncoproteins was similar in darkly pigmented and lightly pigmented heMel cells (fig. S1, C and D). The proliferation and differentiation differences between DMCs and LMCs observed in the untransduced parental cells remained after transduction of the oncoproteins. Darkly pigmented heMel cells proliferated over two times slower than lightly pigmented heMel cells and maintained their more differentiated phenotype (Fig. 1C and fig. S1E),

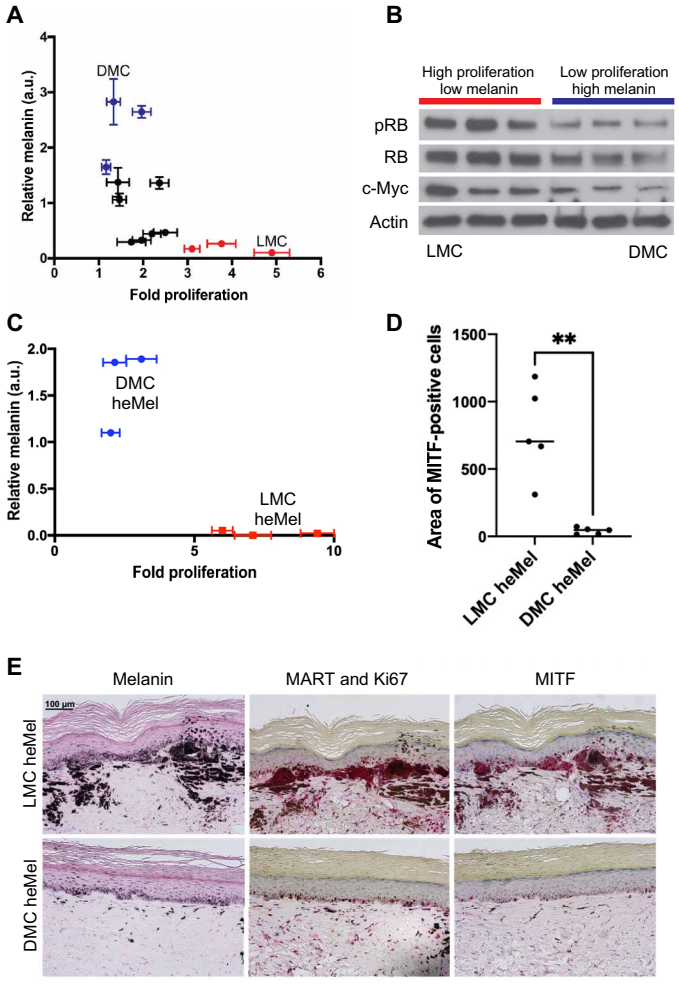

Fig. 1. Cell-intrinsic differences render DMCs less tumorigenic than LMCs. (**A**) Scatterplot of 12 individual primary human MC cultures shows melanin content versus proliferation capacity. (**B**) Western blot of proliferation markers in lightly pigmented MCs (LMCs) and darkly pigmented MCs (DMCs) at baseline. Biologic, $n = 3$. (**C**) Scatterplot of transformed heMel shows melanin content versus proliferation capacity. Biologic, $n = 3$; technical, $n = 3$. (**D**) Quantification of positive epidermal MITF staining area compared to total epidermal area in LMC and DMC heMel samples. $^{**}P = 0.008$ analyzed via *t* test. Images shown are representative fields taken from grafts on five different mice from one biologic replicate of light and dark heMel cells. (**E**) Histologic characterization of representative orthotopic skin and resulting tumors, including MC and proliferation markers MITF (red), Ki67 (dark brown, nuclear)/MART (red), and Fontana Masson (melanin, dark brown). Images taken at ×20 magnification. Scale bar, 100 μm. a.u., arbitrary units.

suggesting that cell-intrinsic factors in DMCs may protect them from the oncogenic effects of common melanoma drivers. These dark and light heMel cells were each heterozygous for melanocortin receptor 1 (MC1R) 163Q, eliminating any potential confounding effects of MC1R polymorphisms. To test whether these in vitro differences translated to different melanoma phenotypes in vivo, lightly and darkly pigmented heMel cells were combined with normal primary human keratinocytes and incorporated into devitalized human dermis to establish three-dimensional skin tissues in organotypic culture (*29*). We then grafted the engineered skin onto the orthotopic location on the backs of severe combined immunodeficient

(SCID) mice. After 100 days, the grafts were harvested and analyzed histologically. Tissues with lightly pigmented heMel cells formed early melanomas, with large proliferative melanocytic nests, defined by MITF and MART staining, and with hallmark melanoma features, including early dermal invasion and upward Pagetoid scatter (Fig. 1, D and E, and fig. S1F). In marked contrast, darkly pigmented heMel cells did not progress to melanoma, although the individual dark heMel cells were present in the basal layer of the epidermis (Fig. 1, D and E, and fig. S1F). We did not observe any spontaneous metastasis to lymph nodes or distant organs over the 3-month experiment. These results show that DMCs resist BRAF-driven transformation, independent of UVR.

DOPA inhibits MC proliferation and melanoma in vitro and in vivo

Although dark MCs contain more pigment than light MCs, eumelanin is a highly insoluble, large heterogeneous polymer without known signaling activity. Therefore, to begin defining the mechanism(s) responsible for reduced proliferation in DMCs, we first looked to upstream intermediates in the melanin synthesis pathway. Melanin is synthesized via a complex multistep process involving serial oxidation and polymerization of tyrosine and is regulated by over 200 different genes (Fig. 2A). Tyrosine is first converted into L-DOPA via Tyr, and this is the rate-limiting step in melanin synthesis (*26*, *30*). Consistent with the premise that Tyr activity increases in parallel with eumelanin content across the human pigment spectrum (*6*, *31*), we detected approximately 300% more DOPA in cultures of primary human DMCs, as compared to LMCs (Fig. 2B).

To test whether DOPA inhibits MC proliferation, we exposed LMCs and DMCs to increasing concentrations of DOPA. DOPA decreased proliferation of LMCs in a dose-responsive and saturable manner, suggesting a specific receptor-mediated activity. In contrast, DOPA had no effect on proliferation of DMCs. DOPA effects in LMCs saturated at 6.25 μM. At this exposure, LMCs proliferated at the same rate as DMCs, suggesting that DMCs contain a saturating amount of endogenously synthesized DOPA (Fig. 2C). Consistent with this, exogenous DOPA supplementation increased melanin synthesis in LMCs but did not affect melanin content in DMCs (fig. S2A).

To determine whether the antiproliferative effect of DOPA is dependent on melanin synthesis, we used the Tyr inhibitor *N*-phenylthiourea (PTU) (*32*–*34*). As Tyr catalyzes not only the reaction of tyrosine to DOPA but also the subsequent conversion of DOPA to dopaquinone (Fig. 2A), PTU prevents conversion of exogenous DOPA to melanin. In LMCs, PTU alone had no significant effect on proliferation, while the combination of PTU and DOPA continued to inhibit cell growth (Fig. 2D and fig. S2B). In DMCs, PTU decreased pigment production and increased proliferation rate. However, DMCs treated with both PTU and DOPA proliferated at the slow baseline DMC rate, although they remained lightly pigmented (Fig. 2D). Together, these data show that DOPA's effects on MC proliferation are independent of melanin, and that differences in endogenously produced DOPA are likely responsible for most, if not all, of the observed proliferation differences between DMCs and LMCs. Moreover, DOPA had no effect on the proliferation of primary human keratinocytes, suggesting that DOPA's effects on proliferation may be unique to MCs (fig. S2C).

In addition to melanin, the biologic impact of DOPA is also generally attributed to its conversion to dopamine and 3-*O*-methyldopa (Fig. 2A), both of which affect activity of dopamine receptors. However, neither of these DOPA metabolites appeared necessary for the antiproliferative effects of DOPA in MCs. We used the DOPA decarboxylase (DDC) inhibitor carbidopa to inhibit the conversion of DOPA to dopamine, and the catechol-*O*-methyltransferase (COMT) inhibitor entacapone to block synthesis of 3-*O*-methyldopa in both primary MCs and A375 melanoma cells. Neither inhibitor nor 3-*O*-methyldopa altered the antiproliferative effect of DOPA (fig. S2, D to H). Also consistent with the idea that dopamine is not a mediator of the observed DOPA effects, liquid chromatography–mass spectrometry (LC-MS) analysis detected minimal amounts of dopamine in MCs, which did not correlate with the melanin content of the cells, whereas DOPA did directly correlate with melanin content (fig. S3A).

To examine whether endogenously produced DOPA in MCs signals via an autocrine-paracrine mechanism, we collected conditioned media from pure MC cultures. Using high-performance LC/MS on conditioned media, we determined that DMCs secrete four to five times more DOPA than LMCs (fig. S3B). We observed that the conditioned media from DMCs reduced LMC proliferation to a rate equal to DMC, and to LMCs treated with DOPA, in a dose-dependent and saturable manner (fig. S3, C and D). Last, we used conditioned media from DMCs treated with PTU to inhibit melanin synthesis and DOPA production, and observed that this significantly ablated the antiproliferative activity in the conditioned media (fig. S3E).

To test whether melanoma cells also respond to DOPA, we treated multiple human and mouse melanoma cell lines with DOPA/carbidopa and observed marked inhibition of proliferation in most, but not all, melanoma lines, independent of BRAF and NRAS mutational status (Fig. 2E and table S1). The mechanism responsible for the observed DOPA resistance is determined below, and these lines thereby proved to be useful for validating our overall conclusion that DOPA effects are mediated by CHRM1. Most of the melanoma cell lines used are Tyr negative, including those that are DOPA responsive, consistent with the idea that DOPA's antiproliferative effect is independent of Tyr and melanin synthesis (fig. S3F).

We next questioned whether DOPA may have therapeutic utility as a systemically delivered agent for melanoma in vivo. Systemic delivery of combined L-DOPA and carbidopa is already Food and Drug Administration (FDA)–approved for Parkinson's disease (*35*). The DOPA/carbidopa combination is used, rather than DOPA alone, because carbidopa inhibits DDC and thereby prevents DOPA from being converted to dopamine everywhere except the brain, where it is needed to treat Parkinson's: Carbidopa does not cross the blood-brain barrier, whereas DOPA does. This combination is therefore ideal for our purposes because we wanted to expose the subcutaneous melanomas to DOPA, but not to dopamine. BL/6 mice harboring syngeneic YUMM1.7 melanoma ($Braf^{V600E/wt}Pten^{-/-}\ Cdkn2^{-/-}$) were treated with a combination of L-DOPA methyl ester (300 mg/kg) and carbidopa (75 mg/kg). Treatment was initiated after tumors reached 2 to 3 mm in diameter (fig. S4A). DOPA/carbidopa treatment was well tolerated by mice and significantly inhibited YUMM1.7 tumor growth (Fig. 2F). To understand whether the L-DOPA and carbidopa treatment effect in this syngeneic model depends on an immune system response to tumor cells, we repeated the experiment using SCID mice and again observed inhibition of tumor growth (fig. S4B). Together, these results suggest that endogenously synthesized DOPA is a major determinant of proliferative differences in MCs and that exogenous DOPA supplementation inhibits melanoma in vivo, independent of an adaptive immune response.

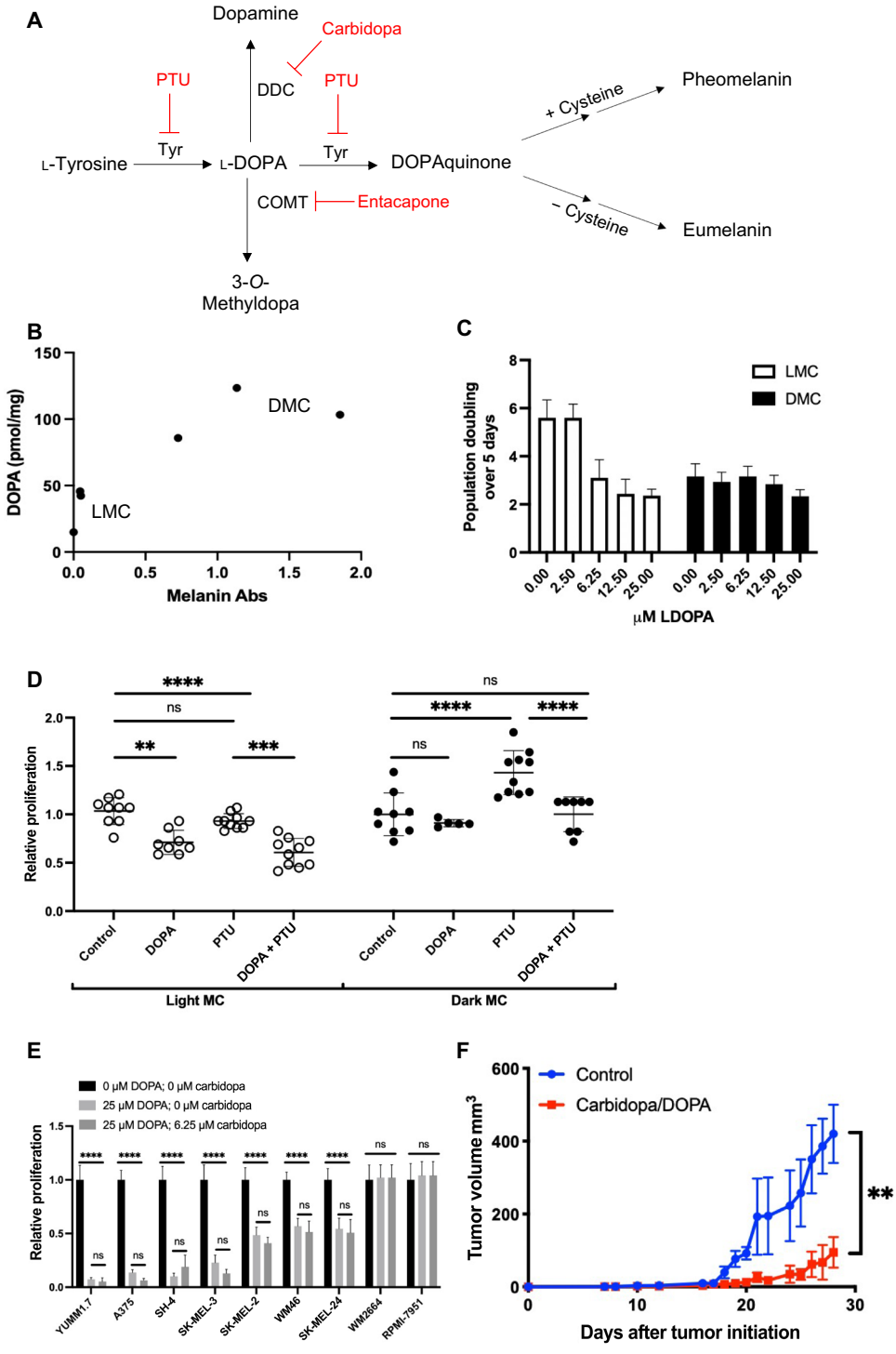

Fig. 2. DOPA inhibits MC proliferation and melanoma in vitro and in vivo. (**A**) Schematic diagram depicting melanin synthesis. Pharmacologic inhibitors used in this paper are shown in red. (**B**) LC-MS quantitation of DOPA content in LMCs and DMCs. Biologic, $n = 3$. (**C**) Dose-response curve of L-DOPA in representative LMC and DMC after 4 days of L-DOPA treatment. Technical, $n = 5$. (**D**) LMCs and DMCs treated with either 25 μM L-DOPA, 75 μM phenylthiourea (PTU), or a combination for 4 days. Image is representative of one biologic replicate of LMC and DMC; technical replicate, $n = 5$. $^{**}P = 0.0033$, $^{***}P = 0.0009$, $^{****}P < 0.0001$ analyzed via two-way analysis of variance (ANOVA). Control populations relative to themselves for both LMC and DMC. (**E**) Panel of melanoma cell lines treated with vehicle, 25 μM L-DOPA, or the combination 25 μM L-DOPA and 6.25 μM carbidopa. $^{****}P < 0.0001$, analyzed via two-way ANOVA. Technical, $n = 5$. (**F**) YUMM1.7 murine melanoma growth in syngeneic BL/6 mice treated with vehicle or L-DOPA methyl ester (300 mg/kg) and carbidopa (75 mg/kg). $^{**}P = 0.0065$. $n = 5$ for each group. ns, not significant.

DOPA antagonizes CHRM1 signaling

Data in Figs. 1 and 2 suggest that DOPA effects in MCs and melanoma cells are specific and receptor mediated. As melanin synthesis and differentiation in MCs are classically regulated by MC1R, a G_s-coupled GPCR, we first considered GPCRs as likely mediators of DOPA effects. To our knowledge, the only previous report associating DOPA with a specific receptor in any cell type identified ocular albinism type 1 (OA1) as a possible DOPA receptor in retina pigment epithelial cells (*36*). To test whether OA1 mediated DOPA effects in melanoma, we depleted OA1 in DOPA-sensitive human melanoma cells using small interfering RNA (siRNA). This had no effect on the DOPA response (fig. S5, A and B). To identify new possible GPCR candidates, we used PRESTO-Tango screening, which is an unbiased high-throughput assay to determine whether DOPA modulates activity of any of the more than 350 nonolfactory human GPCRs (*37*). We compared top hits to genes expressed in MCs and A375 melanoma cells [as determined by RNA sequencing (RNA-seq)] and identified eight GPCRs predicted to be activated by DOPA and nine GPCRs predicted to be inhibited by DOPA (Fig. 3A and files S1 and S2).

Simultaneously, we conducted an in vivo genetic screen in a pigmented human melanoma model using doxycycline (dox)–inducible CRISPR-Cas9 to target all nonolfactory human GPCRs (Fig. 3B and fig. S5, C to E). In this screen, we used injected WM46-Cas9 cells containing the GPCR guide library into SCID mice, which were subsequently fed dox-containing chow to induce Cas9 activity. Tumors were collected after 2 months and sequenced to identify GPCR targets that were selected for or against during melanoma tumorigenesis. Top hits that appeared in both screens were validated via pooled siRNA knockdown of each GPCR receptor in human A375 melanoma cells, as these cells were most highly sensitive to DOPA treatment. The only siRNA pool that rendered cells insensitive to DOPA was the pool targeting CHRM1, a G_q-coupled GPCR (Fig. 3, C and D, and fig. S5A). These complementary pharmacologic and genetic screens therefore converged upon CHRM1, a GPCR not previously known to interact with DOPA, nor to affect melanoma. To further verify results seen with siRNA, we used a complementary CRISPR-Cas9 gene-editing approach with guide RNAs (gRNAs) targeting CHRM1 in A375 melanoma cells. We were unable to achieve complete knockout of CHRM1, likely because of the hypotriploid karyotype of this model and/or the fact that CHRM1 activity promotes proliferation leading to a selection against cells that lose CHRM1. Nonetheless, CRISPR-Cas9–mediated CHRM1 depletion rendered cells much less sensitive to DOPA/carbidopa than the parental cells, indicating that CHRM1 is necessary for the antiproliferative DOPA effects (Fig. 3E and fig. S6A).

Consistent with these data, DOPA responsiveness across a panel of genetically diverse human melanoma cell lines positively correlated with CHRM1 expression, with DOPA-insensitive cells lacking CHRM1 (Fig. 3F and fig. S6B). As DOPA appeared to function as a CHRM1 antagonist, we next tested whether the known CHRM1 synthetic antagonist, pirenzepine (*38*), mimics the observed DOPA effects. In a dose-dependent manner, pirenzepine recapitulated the antiproliferative effects of DOPA/carbidopa treatment in A375 human melanoma. We observed that pirenzepine did not inhibit proliferation in WM2664; however, these cells do not express CHRM1. In contrast, the CHRM1 agonist pilocarpine (*39*) had opposite effects and promoted proliferation in both melanoma cells and DMCs, but again had no response in WM2664 (fig. S6, C to E). The endogenous CHRM1 agonist is acetylcholine (ACh). Although we did not detect ACh in primary MC cultures in vitro, ACh from nonneuronal sources is abundant in human skin (*40*–*42*). ACh promoted proliferation of DMCs, but not LMCs, and this effect was inhibited by DOPA treatment (fig. S6, F and G). Together, these data demonstrate that CHRM1 activation promotes MC and melanoma cell proliferation, CHRM1 is necessary for the antiproliferative effects of DOPA, and DOPA inhibits the pro-proliferative activity of the endogenous CHRM1 agonist ACh.

To determine whether CHRM1 expression is sufficient to confer DOPA sensitivity to DOPA-insensitive melanoma cells lacking CHRM1, we used lentiviral transduction to express CHRM1 in two nonresponding melanoma cell lines, RPMI-7951 and WM2664. Upon CHRM1 expression, cells grew faster than parental controls, suggesting that CHRM1 may promote melanoma (Fig. 3, G and H). In published data from clinical samples (*43*), high CHRM1 expression in melanoma is correlated with decreased overall survival and increased stage progression (fig. S7, A and B). CHRM1 expression rendered RPMI-7951 and WM2664 newly sensitive to DOPA, supporting the idea that CHRM1 is both necessary and sufficient for DOPA effects in MC and melanoma. To further confirm the specificity of these genetic and pharmacologic data, and to control for possible off-target effects of the CHRM1 targeting gRNA, we used lentiviral transduction to restore CHRM1 expression in A375 cells, in which we had previously depleted CHRM1 using CRISPR-Cas9. With this transgene rescue, cells were resensitized to DOPA (fig. S7, C and D). Together, these data show that CHRM1 is a major mediator of DOPA effects in melanoma.

DOPA inhibits G_q signaling and represses FOXM1

The PRESTO-Tango screen indicates that DOPA inhibits CHRM1 signaling. To validate that DOPA inhibits CHRM1 signaling, we next used diacylglycerol (DAG) fluorescent biosensors (*44*). Upon activation of G_q-coupled GPCRs, phospholipase C (PLC) cleaves phosphatidylinositol 4,5-bisphosphate (PIP_2) to form DAG and inositol triphosphate (IP_3). Therefore, changes in DAG are direct readouts of G_q signaling. In this assay, exogenous ACh rapidly increased DAG and this effect was markedly attenuated in the presence of DOPA (Fig. 4A). In cells treated with ACh alone, CHRM1 refired upon subsequent exposure to ACh. However, CHRM1 refiring was markedly inhibited in cells exposed to a combination of DOPA and ACh, indicating that DOPA inhibits CHRM1 signaling and promotes CHRM1 desensitization (Fig. 4A). DOPA alone did not induce a change in DAG. Similar changes in DAG were also observed with pirenzepine, a well-known synthetic CHRM1 antagonist (fig. S8A). Together, these data show that DOPA inhibits CHRM1 G_q-coupled signaling.

G_q-coupled signaling activates both Ras/mitogen-activated protein kinase (MAPK) and phosphoinositide 3-kinase (PI3K)/AKT downstream signaling in other cell types (*45*–*47*). Both of these pathways are major drivers of melanoma and other cancers and are targets of approved inhibitors used clinically (*48*, *49*). Consistent with our discovery that CHRM1 is a DOPA-sensitive melanoma driver, exogenous DOPA induced rapid depletion of both phosphorylated extracellular signal–regulated kinase (ERK) and phosphorylated AKT in melanoma cells (fig. S8B). Exogenous DOPA also led to FOXM1 depletion in DOPA-responsive cell lines (A375 and SH4) but did not deplete FOXM1 in cell lines lacking CHRM1 (RPMI-7951 and WM2664) (Fig. 4, B and C, and fig. S8, C to F). In parallel with FOXM1 depletion, we observed c-Myc loss (Fig. 4C and fig. S8F). FOXM1 and c-Myc both function as transcription factors and proliferation

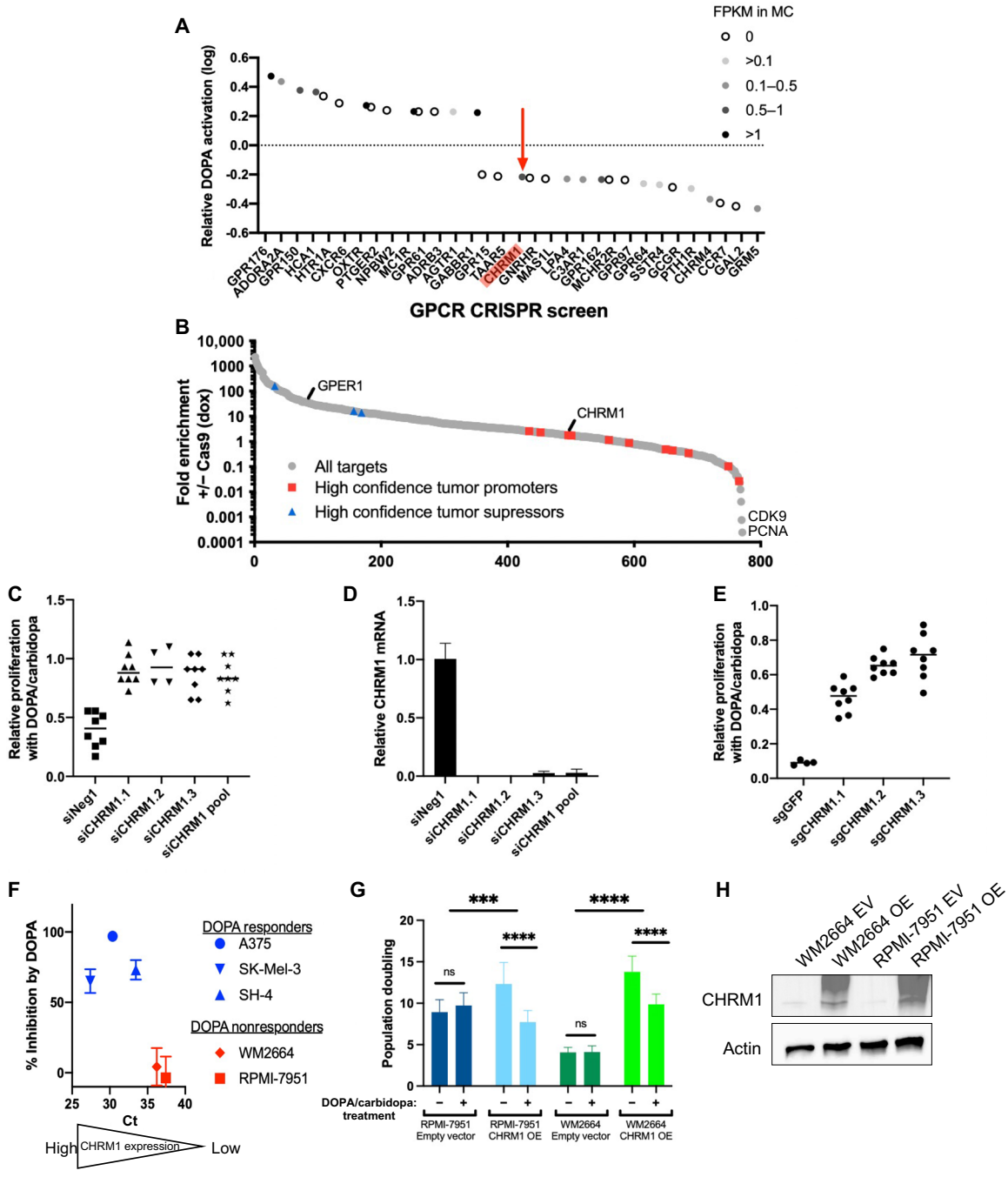

Fig. 3. DOPA antagonizes CHRM1. (**A**) DOPA-mediated GPCR activation or inhibition as determined by the PRESTO-Tango reporter assay. Data points are shaded on the basis of relative expression determined using RNA-seq in MCs (FPKM). (**B**) Log fold enrichment of CRISPR gRNAs selected for or against. Controls for protumorigenic proteins included CDK9 and PCNA. GPER1 served as an internal GPCR tumor suppressor control. High-confidence hits are targets with at least five guides that are selected for (>5-fold) or against (<0.1-fold), and where those five guides represent at least 50% of total guides for that gene. (**C**) siRNA-mediated CHRM1 depletion in A375 human melanoma in the presence of 25 μM L-DOPA and 6.25 μM carbidopa after 5 days of treatment. Technical, $n = 8$. (**D**) qPCR for CHRM1 mRNA in A375 after siRNA treatment confirming knockdown. Time point taken 24 hours after siRNA transfection. Technical, $n = 3$. (**E**) Effect of 25 μM L-DOPA and 6.25 μM carbidopa on proliferation of A375 cells in which CHRM1 was depleted using CRISPR-Cas9 versus control gRNA against green fluorescent protein (GFP). Cell number was determined at day 5. Technical, $n = 8$. (**F**) Low CHRM1 expression, determined via qPCR, correlates with lack of response to 25 μM L-DOPA and 6.25 μM carbidopa. $n = 3$. (**G**) CHRM1 overexpression (OE) in WM2664 and RPMI-7951 human melanoma (DOPA nonresponders) in the presence or absence of 25 μM L-DOPA and 6.25 μM carbidopa after 5 days of treatment. ***$P = 0.0002$, ****$P < 0.0001$ analyzed via two-way ANOVA. $n = 5$. (**H**) Western blot for CHRM1 in WM2664 and RPMI-7951 after transduction with either empty vector or CHRM1.

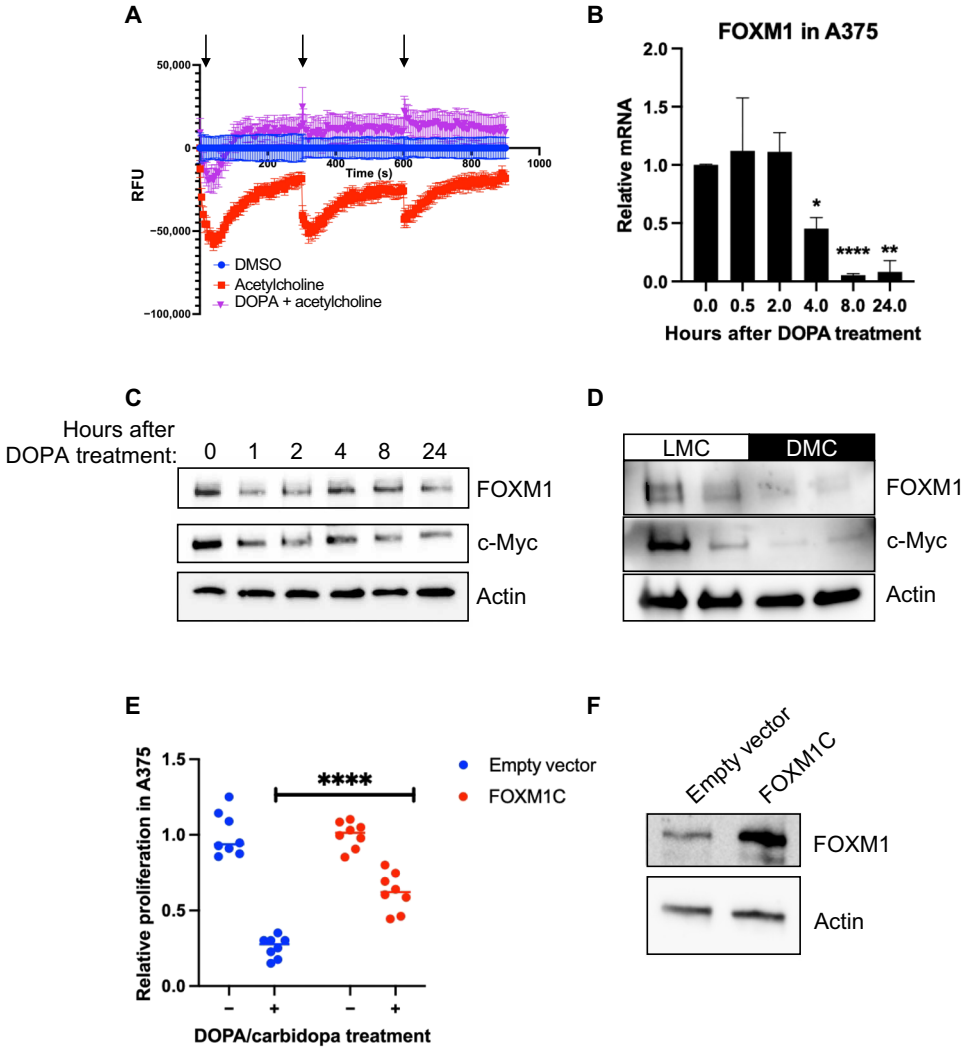

Fig. 4. DOPA inhibits Gq signaling and represses FOXM1. (**A**) Relative fluorescence intensity (RFU) of diacylglycerol (DAG) sensor in HEK293T upon addition of 5 nM ACh or combination of 100 μM DOPA and 5 nM ACh. Cells treated with combination of 100 μM DOPA and 5 nM ACh were pretreated with 100 μM DOPA 1 hour before plate reading. Drugs injected where arrows are pointed. $n = 10$. (**B**) FOXM1 mRNA level determined over time via qPCR in A375 human melanoma treated with 25 μM L-DOPA and 6.25 μM carbidopa. *$P = 0.0142$, **$P = 0.0054$, ****$P < 0.0001$. $n = 3$. (**C**) Western blot for FOXM1 and c-Myc in lysates from A375 human melanoma cells treated with 25 μM L-DOPA and 6.25 μM carbidopa. (**D**) Western blot of FOXM1 and c-Myc at baseline in light and dark MCs. Biologic, $n = 2$ for LMC and DMC. (**E**) Proliferation in A375 cells following transduction with FOXM1C versus empty vector ± 25 μM L-DOPA and 6.25 μM carbidopa. ****$P < 0.0001$. $n = 8$. (**F**) Western blot confirming FOXM1C overexpression in A375 human melanoma.

drivers positively regulated by MAPK and AKT (*50*–*54*). We also found that LMCs, which synthesize less endogenous DOPA than DMCs, contain higher levels of FOXM1 protein (Fig. 4D and fig. S8G).

We were specifically interested in this DOPA-induced FOXM1 depletion as FOXM1 is overexpressed in up to 70% of metastatic melanomas and high expression correlates with worse outcomes (*51*, *55*, *56*). FOXM1 stimulates cell growth by promoting genes critical for cell proliferation and is a key regulator of the G_1-S phase transition. To examine whether FOXM1 loss was necessary for the antiproliferative effects of DOPA, we overexpressed FOXM1C, the primary isoform in MCs and melanoma (*51*). This attenuated, but did not completely abolish, DOPA's antiproliferative effect (Fig. 4, E and F).

Pharmacologic inhibition of FOXM1 suppresses melanoma growth

Encouraged by our data showing that FOXM1 loss downstream of CHRM1 was necessary for the antiproliferative effects of DOPA, we next questioned whether FOXM1 inhibition alone was sufficient to similarly inhibit melanoma proliferation (Fig. 5). Historically, transcription factors have been viewed as generally undruggable targets (*57*). However, small-molecule inhibitors that block DNA binding have recently been developed for FOXM1 (*58*). In vitro exposure to the FOXM1 inhibitor FDI-6 markedly reduced melanoma cell proliferation and, most notably, included a marked change in melanoma cell morphology: Cells became multipolar and larger, and generally appeared more like normal primary MCs than the untreated melanoma cells, which had a rounded/oval appearance (Fig. 6, A and B,

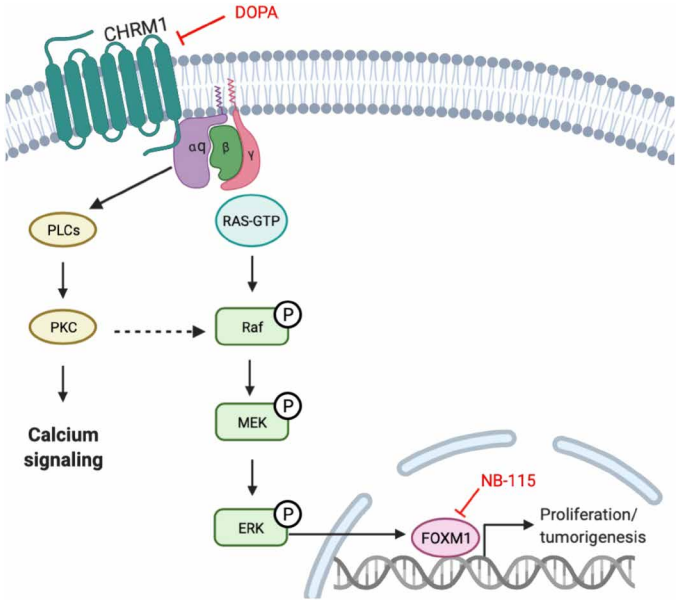

Fig. 5. Schematic overview of CHRM1 signaling in melanoma. Proposed mechanism of oncogenic CHRM1 signaling in melanoma. Red text denotes inhibitors of this pathway used in this manuscript.

and fig. S9A). These morphologic features have also been recognized by others as indicative of a more fully differentiated MC cell state (*59*). Consistent with this idea, LMCs were more sensitive to FDI-6 treatment than DMCs (fig. S9B).

While FDI-6 shows promising results in vitro and is a useful and readily available research tool, it has very poor pharmacokinetic properties and is not useful for in vivo studies (*60*). However, a new class of FOXM1 inhibitors was recently shown to have activity in preclinical breast cancer models, without significant systemic toxicity (*60*). Three of these new FOXM1 inhibitors—NB-55, NB-73, and NB-115—were more effective than FDI-6 at inhibiting melanoma proliferation (Fig. 6C). Consistent with the idea that FOXM1 is a critical element downstream of CHRM1, NB-115 inhibited cell growth in a variety of human and mouse melanoma cell lines, including those that do not respond to DOPA because they lack CHRM1. NB-115–mediated FOXM1 depletion was associated with depletion of FOXM1 protein itself, as well as depletion of c-Myc (Fig. 6, D and E, and fig. S9, C to E). FOXM1 and c-Myc are both known to positively regulate the transcription of each other (*61*, *62*), and the observed loss of FOXM1 agrees with previous reports establishing that NB-55, NB-73, and NB-115 promote proteasome-mediated FOXM1 degradation (*60*).

We next tested whether systemically delivered NB-115 inhibited melanoma in vivo. BL/6 mice harboring syngeneic YUMM1.7 melanoma ($Braf^{V600E/wt}Pten^{-/-}$ $Cdkn2^{-/-}$) were treated with NB-115 (6 mg/kg). This significantly inhibited YUMM1.7 melanoma growth and extended overall survival, with one mouse completely clearing its tumor (Fig. 6, F and G). Together, these data suggest that CHRM1 is a melanoma target that is regulated by DOPA, which is naturally synthesized in MCs. Further, FOXM1 is a critical downstream regulator of DOPA's antiproliferative effect and itself appears to be a potential therapeutic target.

DISCUSSION

Decades of clinical and epidemiological data suggest that the physical UV shielding effect of eumelanin (brown-black) is insufficient to fully explain the difference in melanoma incidence between lightly and darkly pigmented skin. While eumelanin is known to have a protective effect against melanoma, studies have shown that pheomelanin (yellow-red) may have an opposite effect that accelerates the progression of UV-independent melanoma (*63*). However, it is unlikely that pheomelanin is responsible for the different proliferation and cancer susceptibility phenotypes shown here between LMC and DMC, as the total amount of pheomelanin is generally constant across skin pigment types; instead, skin pigmentation is determined primarily by differences in relative eumelanin (*64*). We posit that the mechanisms responsible for the differences in proliferation rate that we routinely observe between LMC and DMCs also contribute to the associated differences in melanoma susceptibility. To our knowledge, this is the first work to directly explore UV-independent cell-intrinsic signaling differences between human LMC and DMC, first to show that CHRM1 signaling is inhibited by DOPA, first to establish a role for CHRM1 in MC homeostasis, and first to demonstrate that CHRM1 and FOXM1 are potential therapeutic targets for melanoma. We cannot formally establish from these data whether DOPA directly interacts with CHRM1 versus with a component of a CHRM1 complex; distinguishing between these is difficult and may not be resolvable even with traditional radioligand binding studies. Cryo–electron microscopy may be able to further refine the structural molecular mechanisms by which DOPA inhibits CHRM1 signaling. Future research and clinical trials involving MCs and melanoma may benefit from consideration of the baseline eumelanin content of the cells, as differences in DOPA and CHRM1 signaling are likely to affect some of the experimental results and the corresponding interpretation.

Our data are consistent with some provocative but mechanistically unexplained findings from older literature. DOPA was shown 30 years ago to bind to a protein in rodent melanoma cell membranes, although the specific protein was not identified, and the functional consequences of that binding for MC function or melanoma pathology were not determined (*65*, *66*). In addition, studies have identified L-DOPA as a regulator of MC functions, although the mechanism(s) responsible was not established (*67*, *68*). Even more tantalizing, 45 years ago, L-DOPA methyl ester was shown to inhibit B16 melanoma in mice, but whether that resulted from DOPA itself, melanin, or other metabolite was not determined. We show that many DOPA-responsive melanoma cell lines lack Tyr and are unpigmented, further suggesting that DOPA itself and not eumelanin or another downstream metabolite is responsible for the antiproliferative effect. Most critically, the receptor and signaling mechanism(s) mediating that DOPA effect in those older studies were not determined, and those observations appear to be mostly forgotten in recent melanoma literature (*69*–*71*). We establish here that (i) DOPA effects are mediated via autocrine/paracrine inhibition of CHRM1 signaling, which contributes to UV-independent differences between LMCs and DMCs, (ii) that CHRM1 is necessary for the antiproliferative DOPA effect, and (iii) that expression of a CHRM1 transgene is sufficient to confer DOPA sensitivity in DOPA-insensitive, CHRM1-lacking melanoma lines. We primarily relied on quantitative polymerase chain reaction (qPCR) to determine endogenous CHRM1 expression in nonresponsive cells as detecting endogenous CHRM1 protein by Western blotting is challenging;

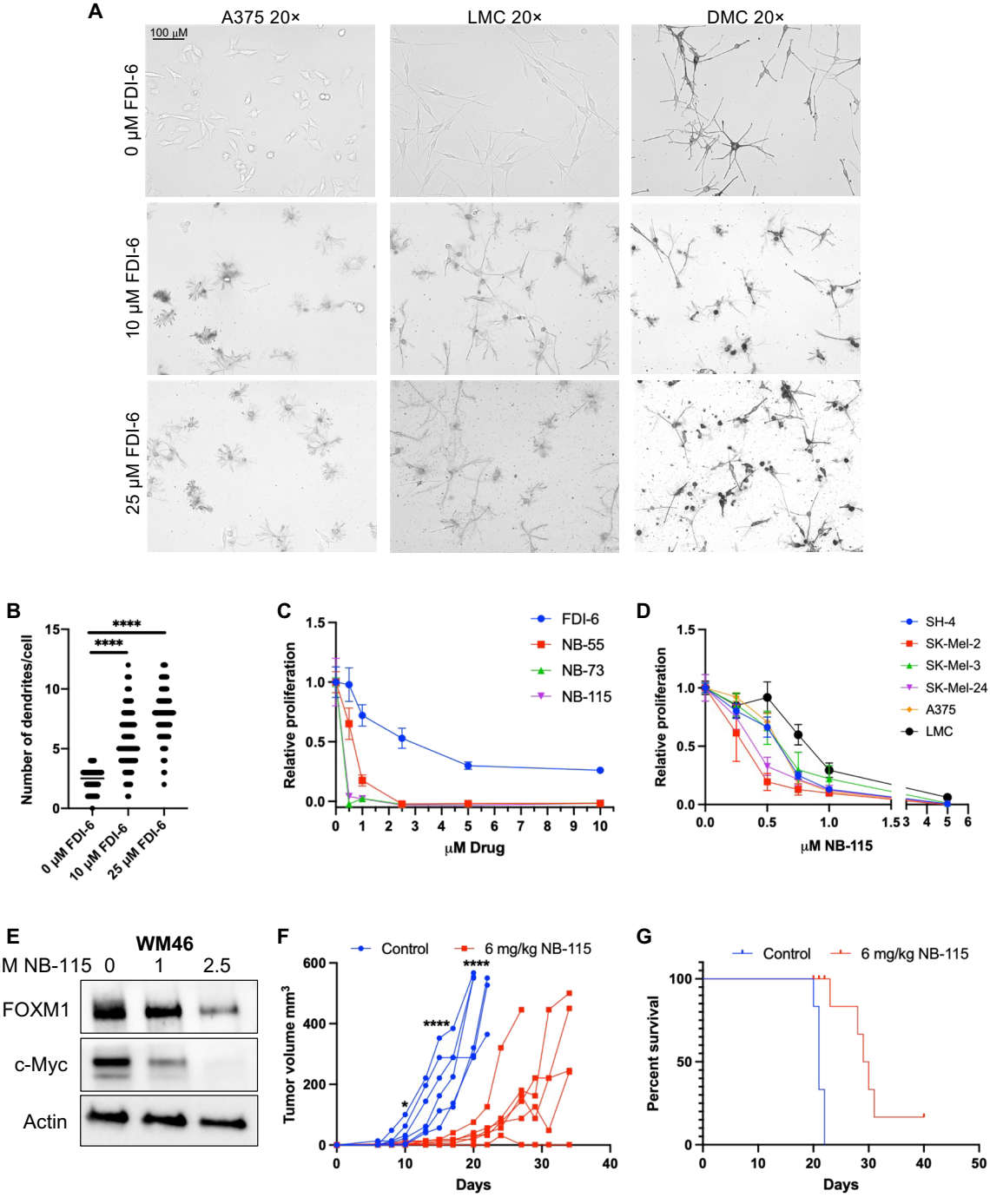

Fig. 6. Pharmacologic FOXM1 inhibition suppresses melanoma growth and extends animal survival. (**A**) Morphologic appearance of A375 human melanoma, LMCs, and DMCs after 24 hours of exposure to increasing concentrations of FDI-6 (FOXM1i). ****$P < 0.0001$ analyzed via *t* test. Images of one replicate, $n = 3$. (**B**) Change in number of dendrites per A375 cell after exposure to FDI-6 for 24 hours. Ten representative fields at ×10 magnification from each condition were quantified. (**C**) Proliferation of A375 human melanoma cells in the presence of increasing concentrations of FOXM1 inhibitors, including FDI-6 (commercially available), NB-55, NB-73, and NB-115. Cell proliferation assay using WST-8 cell viability dye. $n = 5$. (**D**) Proliferation of a panel of melanoma cell lines in the presence of increasing concentrations of NB-115. $n = 5$. (**E**) FOXM1 and c-Myc protein in WM46 human melanoma after exposure to NB-115 for 24 hours. (**F**) YUMM1.7 melanoma growth over time in BL/6 mice treated with vehicle or NB-115 (6 mg/kg). $N = 6$ for each group across two identical experiments. *$P = 0.0117$, ****$P < 0.0001$ by two-way ANOVA. (**G**) Survival probability over time of mice treated with vehicle or NB-115 (6 mg/kg). $N = 6$ for each group across two identical experiments. ****$P < 0.0001$, Mantel-Cox test.

GPCRs are generally expressed at low levels, and there are a very limited number of antibodies available. While a commercially available antibody was sufficient to detect an overexpressed CHRM1 in our studies, it was not sufficiently specific to reliably distinguish low-level, endogenous CHRM1 from nonspecific bands in all of the melanoma lines used. However, in A375 human melanoma cells, we were able to detect a significant decrease in the intensity of the CHRM1 band in cells with CRISPR-Cas9–mediated CHRM1 depletion.

ACh, which is abundantly available in human skin (*40*, *41*), signals through the muscarinic ACh receptors (mAChRs), including CHRM1, and these receptors have been shown to be present in normal human MCs (*72*). Signaling through mAChRs affects a wide spectrum of diseases, and hence, many mAChR antagonists are already approved in the United States for use in people. Among these are atropine for childhood myopia (*73*) and scopolamine for motion sickness (*74*). Unfortunately, these agents have very short half-lives in vivo and are thereby not suitable for cancer studies. Nonetheless, we have shown that future mAChR antagonists with improved systemic pharmacokinetic properties may be effective against melanoma. Although cholinergic muscarinic receptors are best known for their activity in the nervous system, ours is not the first work to implicate ACh in cancer progression, as recent work in murine prostate cancer models established that the nerves activate protumorigenic cholinergic signaling in the tumor microenvironment that promotes tumor invasion and metastasis (*75*).

We showed that combination treatment of DOPA and carbidopa, an FDA-approved therapy for Parkinson's disease, mimics the effects of endogenously produced DOPA in DMCs and thereby inhibits melanoma. Parkinson's disease is a neurodegenerative disorder caused by a loss of dopaminergic neurons in the substantia nigra, ultimately leading to a decline in motor function. Multiple epidemiological studies have found an association between melanoma and Parkinson's disease (*76*–*78*). This association is reciprocal: Patients with melanoma have an increased risk of Parkinson's disease, and patients with Parkinson's disease are more likely to develop melanoma. Studies have also shown that incidence in Parkinson's disease is two to three times more common in white populations as compared to African-American populations (*79*, *80*). These epidemiological studies, together with this current work, suggest that the relative lack of DOPA in lightly pigmented individuals may predispose them not only to melanoma but also to Parkinson's; however, the pathobiology of Parkinson's disease is complex, and further investigation is needed to determine whether these two seemingly disparate diseases are mechanistically linked through DOPA.

Last, we established that pharmacologic DOPA/carbidopa led to decreased activation of both the MAPK and AKT pathways and ultimately down-regulation of FOXM1, a major cancer driver (*56*). While FOXM1 is downstream of both the MAPK and AKT pathways, FOXM1 depletion is unlikely to be the sole mechanism by which DOPA inhibits melanoma, as FOXM1 overexpression only partially rescued cell proliferation in the presence of exogenous DOPA. This could be because of the c-Myc protein depletion we observe following DOPA exposure and/or to DOPA-induced changes in other tumor-potentiating proteins. Nonetheless, selective pharmacologic FOXM1 inhibition significantly inhibited proliferation of all melanoma lines tested in vitro and in vivo, independent of CHRM1 status, suggesting that FOXM1 may be a more generalizable melanoma therapeutic target. Moreover, NB-115 is potentially more efficacious than DOPA against melanoma, as we observed some YUMM1.7 tumors clear completely with NB-115, which we did not observe with DOPA. Future studies will be needed to determine whether the utility of this new class of FOXM1 inhibitors extends to noncutaneous melanoma and other cancers. Together, this work demonstrates how the natural genetic diversity in humans can be used as a window to discover previously undefined signaling pathways regulating normal tissue homeostasis and carcinogenesis.

MATERIALS AND METHODS

Cell culture and proliferation assays

Primary human MCs, keratinocytes, and fibroblasts were extracted from fresh discarded human foreskin and surgical specimens as previously described (*22*, *29*). All human cells obtained from the University of Pennsylvania Skin Biology and Disease Research Core (SBDRC) were isolated from deidentified discarded tissue and therefore considered to be IRB (Institutional Review Board) exempt by our institution and the National Institutes of Health (NIH). Keratinocytes were cultured in a 1:1 mixture of Gibco Keratinocytes-SFM medium + L-glutamine + epidermal growth factor (EGF) + BPE (bovine pituitary extract) and Gibco Cascade Biologics 154 medium with 1% penicillin-streptomycin (Thermo Fisher Scientific, #15140122). Fibroblasts were cultured in Dulbecco's modified Eagle's medium (DMEM; Mediatech, Manassas, VA, USA) with 5% fetal bovine serum (FBS; Invitrogen, Carlsbad, CA, USA) and 1% penicillin-streptomycin. Primary MCs and human-engineered melanoma cells (heMel) were cultured in Medium 254 (Thermo Fisher Scientific, #M254500) with 1% penicillin-streptomycin.

YUMM1.7, SH-4, and SK-MEL-2 cells were purchased from the American Type Culture Collection (ATCC) (YUMM1.7 ATCC CRL-3362; SH-4 ATCC CRL-7724; SK-MEL-2 ATCC HTB-68) and cultured in DMEM with 5% FBS and 1% penicillin-streptomycin. SK-MEL-3 cells were purchased from ATCC (ATCC HTB-69) and cultured in McCoy's 5A (modified) medium with 15% FBS (Invitrogen, Carlsbad, CA, USA) and 1% penicillin-streptomycin. RPMI-7951 and SK-MEL-24 cells were purchased from ATCC (RPMI-7951 ATCC HTB-66; ATCC HTB-71) and cultured in Eagle's minimum essential medium with 15% FBS and 1% penicillin-streptomycin. WM46 and WM2664 melanoma cells were a gift from M. Herlyn (Wistar Institute, Philadelphia, PA, USA) and were cultured in TU2% media. Tumor cells were regularly tested using the MycoAlert Mycoplasma Detection Kit from Lonza (Allendale, NJ, USA).

For monitoring cell proliferation, 10×10^5 YUMM1.7 or A375, 12×10^5 RPMI-7951, 15×10^5 WM46, WM2664, SH4, SK-MEL-2, SK-MEL-24, or SK-MEL-3, or 30×10^5 MCs were seeded per well in 12-well cell culture plates. Cells were treated every second day and manually counted in triplicate using a hemocytometer. All the experiments were performed in cell populations that were in culture during a maximum of 3 weeks (five passages in average) since thaw from the corresponding stock. Fold proliferation was calculated by counting cells after 4 days of proliferation and dividing the final cell number by the starting cell number. Experiments with primary human MCs were completed with at least two biologic replicates of either LMC or DMC.

3,4-Dihydoxy-L-phenylalanine (D9628), PTU (P7629), and FDI-6 (SML1392) were purchased from Sigma-Aldrich (St. Louis, MO, USA). (*S*)-(−)-Carbidopa (0455), pirenzepine dihydrochloride (1071), and pilocarpine hydrochloride (0694) were purchased from Tocris Bioscience (Bristol, UK). 3-*O*-methyl-L-DOPA hydrate (20737) and

entacapone (14153) were purchased from Cayman Chemicals (Ann Arbor, MI, USA). NB-55, NB-73, and NB-115 were prepared as described (*60*).

Genetic manipulation of CHRM1

We used lentiviral transduction to deliver dox-inducible Cas9 and gRNA targeting CHRM1 in human A375 melanoma cells. Three different gRNAs were used to target CHRM1. Transduced cells were selected with puromycin, and single cells were subsequently isolated, expanded, and examined for CHRM1 protein expression, compared to clones isolated in parallel with no dox treatment. The following gRNA sequences were used (5′-3′): sgCHRM1.1_Fw, caccgGCTCCGAGACGCCAGGCAAA; sgCHRM1.1_Rv, aaacTTTGCCTGGCGTCTCGGAGCc; sgCHRM1.2_Fw, caccgGATGCCAATGGTGGACCCCG; sgCHRM1.2_Rv, aaacCGGGGTCCACCATTGGCATCc; sgCHRM1.3_Fw, caccgCAAGCGGAAGACCTTCTCGC; sgCHRM1.3_Rv, aaacGCGAGAAGGTCTTCCGCTTGc.

Using Thermo Fisher Scientific's Silencer Silect protocol, we knocked down CHRM1 in human A375 melanoma cells. Briefly, each siRNA was diluted in Opti-MEM (Invitrogen, 31985062) to a concentration of 10 μM, to ultimately be diluted to 30 pmol in a six-well plate. If siRNAs were pooled, each individual siRNA was used at 10 pmol (for a combined total of 30 pmol) in a six-well plate. Diluted siRNAs were combined with diluted Lipofectamine (Invitrogen, 11668027) and incubated on cells for 24 hours. After 24 hours, cells were plated in a 12-well plate with 10,000 cells per well and treated with a combination of DOPA and carbidopa for 4 days.

We used three different siRNAs against CHRM1: s3023 (labeled siCHRM1.1), s3024 (labeled siCHRM1.2), and s553080 (labeled siCHRM1.3). Negative controls included Negative Control No. 1 (Thermo Fisher Scientific, 4390843) and Negative Control No. 2 (Thermo Fisher Scientific, 4390846) and a positive control against Kif11 (University of Pennsylvania, High-throughput sequencing core).

CHRM1 overexpression vector was cloned from a codon-optimized plasmid available on Addgene (plasmid no. 66248). As the Addgene plasmid was a CHRM1 fusion protein, a stop codon was introduced to produce CHRM1 at the correct size, which was then cloned into the PRRL vector. The PRRL-CHRM1 plasmid was sequenced to confirm the correct sequence, including the stop codon, and the plasmid was redigested to confirm the correct band size.

Genetic manipulation of FOXM1

We used lentiviral transduction to deliver the FOXM1C plasmid into cells. Construct was purchased from Addgene (plasmid no. 68810). As expression was inducible, cells were grown in dox for 3 days when overexpression was confirmed before proliferation assays.

Human-engineered melanoma xenografts

Organotypic skin grafts were established using modifications to previously detailed methods (*22*, *29*). The keratinocyte growth medium (KGM) used for keratinocyte-only skin grafts was replaced with modified melanocyte xenograft seeding medium (MXSM). MXSM is a 1:1 mixture of KGM, lacking cholera toxin, and keratinocyte medium 50/50 (Gibco) containing 2% FBS, 1.2 mM calcium chloride, 100 nM Et-3 (endothelin 3), recombinant human stem cell factor (10 ng/ml), and recombinant basic fibroblast growth factor (4.5 ng/ml). Briefly, primary human MCs were transduced with lentivirus carrying BRAF(V600E), dominant-negative p53(R248W), active CDK4(R24C), and hTERT. Transduced MCs (1×10^5 cells) and keratinocytes (5×10^5 cells) were suspended in 80 μl of MXSM, seeded onto the dermis, and incubated at 37°C for 4 days at the air-liquid interface to establish organotypic skin. Two biologic replicates of light heMel cells and two biologic replicates of dark heMel cells were used for xenograft experiments. Organotypic skin tissues were grafted onto 5- to 7-week-old female ICR SCID mice (Taconic) according to an International Animal Care and Use Committee (IACUC)–approved protocol at the University of Pennsylvania. Mice were anesthetized in an isoflurane chamber, and murine skin was removed from the upper dorsal region of the mouse. Organotypic human skin was reduced to a uniform 11 mm by 11 mm square and grafted onto the back of the mouse with individual interrupted 6-0 nylon sutures. Mice were dressed with Bactroban ointment, Adaptic, Telfa pad, and Coban wrap. Dressings were removed 2 weeks after grafting. Mice were sacrificed 100 days after grafting, and organotypic skin was removed for histology.

Subcutaneous tumors and treatments

All mice were purchased from Taconic Biosciences Inc. (Rensselaer, NY, USA). These studies were performed without inclusion/exclusion criteria or blinding but included randomization. On the basis of a twofold anticipated effect, we performed experiments with at least five biological replicates. All procedures were performed in accordance with IACUC-approved protocols at the University of Pennsylvania. Subcutaneous tumors were initiated by injecting 10×10^5 YUMM1.7 cells in 50% Matrigel (Corning, Bedford, MA, USA) into the subcutaneous space on the left or right flanks of mice. For all tumor experiments, tumors grew for 1 week until about 2 mm by 2 mm in size before drug injections were started. For L-DOPA and carbidopa experiments, L-DOPA methyl ester (300 mg/kg; Tocris, #0455) and carbidopa (75 mg/kg; Cayman, #16149) were injected intraperitoneally daily for 3 weeks, then 5 days on and 2 days off for the remainder of the experiment. In the SCID mouse experiment, drugs were injected 3 days on and 1 day off for the entire experiment. Both drugs were resuspended in normal saline. Carbidopa was injected 1 hour before L-DOPA injection. For FOXM1 inhibitor experiments, NB-115 (6 mg/kg) was injected subcutaneously every other day. NB-115 was dissolved in dimethyl sulfoxide and diluted 1:10 in sesame oil to form a stable, homogeneous suspension. As subcutaneous tumors grew in mice, perpendicular tumor diameters were measured using calipers. Volume was calculated using the formula $L \times W^2 \times 0.52$, where L is the longest dimension and W is the perpendicular dimension. Animals were euthanized when tumors exceeded a protocol-specified size of 500 mm^3. Secondary endpoints include severe ulceration, death, and any other condition that falls within the IACUC guidelines for Rodent Tumor and Cancer Models at the University of Pennsylvania.

Western blot analysis

Adherent cells were washed once with DPBS (Dulbecco's Phosphate Buffered Saline) and lysed with 8 M urea containing 50 mM NaCl and 50 mM tris-HCl (pH 8.3), 10 mM dithiothreitol, and 50 mM iodoacetamide. Lysates were quantified (Bradford assay), normalized, reduced, and resolved by SDS gel electrophoresis on 4 to 15% tris/glycine gels (Bio-Rad, Hercules, CA, USA). Resolved protein was transferred to polyvinylidene difluoride membranes (Millipore, Billerica, MA, USA) using a semi-dry transfer cell (Bio-Rad), blocked in 5% bovine serum albumin in TBS-T (Tris-buffered saline with 0.1% Tween 20 detergent), and probed with primary antibodies

recognizing β-actin (Cell Signaling Technology, #3700, 1:4000, Danvers, MA, USA), c-Myc (Cell Signaling Technology, #5605, 1:1000), p-RB (phosphorylated-retinoblastoma protein) S807/811 (Cell Signaling Technology, #8516, 1:1000), RB (retinoblastoma protein) (Cell Signaling Technology, #9313, 1:1000), p-CREB S133 (Cell Signaling Technology, #9198, 1:1000), CREB (Cell Signaling Technology, #9104, 1:1000), Tyr (Abcam, T311, 1:1000), p53 (Cell Signaling Technology, #2527, 1:1000), CDK4 (Cell Signaling Technology, #12790, 1:1000), P-ERK [Cell Signaling Technology, p-p44/42 MAPK (Erk1/2) (Thr^{202}/Tyr^{204}) (D13.14.4E) XP rabbit monoclonal antibody (mAb) #4370, 1:1000], ERK [Cell Signaling Technology, p44/42 MAPK (Erk1/2) (137F5) rabbit mAb #4695, 1:1000], pAKT S473 (Cell Signaling Technology, #9271, 1:1000), AKT (Cell Signaling Technology, #9272, 1:1000), CHRM1 (Invitrogen, #PA5-95151, 1:1000), FoxM1 (Cell Signaling Technology, #5436, 1:1000), and $BRAF^{V600E}$ (Sigma-Aldrich, #SAB5600047, 1:1000). After incubation with the appropriate secondary antibody, proteins were detected using either Luminata Crescendo Western HRP Substrate (Millipore) or ECL Western Blotting Analysis System (GE Healthcare, Bensalem, PA). After incubation with the appropriate secondary antibody [rabbit anti-mouse immunoglobulin G (IgG) H&L (Biotin) preadsorbed (ab7074); anti-mouse IgG, horseradish peroxidase (HRP)–linked antibody, #7076, 1:2000], proteins were detected using Clarity Western ECL Substrate (Bio-Rad, #170–5060). All Western blots were repeated at least three times. Quantification of Western blots was completed using ImageJ software. All bands were compared relative to actin loading control to determine "Relative Protein Level."

Quantitative RT-PCR

RNA was extracted using RNeasy kit (Qiagen, #74104) following the manufacturer's instructions. cDNA was obtained using the High Capacity cDNA Reverse Transcription Kit (Applied Biosystems, #4368814). For quantitative real-time PCR, PowerUP SYBR Green Master Mix (Applied Biosystems, #A25741) was used. ViiA 7 Real-Time PCR System was used to perform the reaction (Applied Biosystems). Values were corrected by β-actin expression. The $2^{-\Delta\Delta Ct}$ method was applied to calculate the relative gene expression. Primers used are included in table S2. β-Actin primers have been previously published in papers by our laboratory [PMID (PubMed Reference number), 34706862]. FOXM1 and hTERT primers were previously published (PMID, 17392427 and 22854964). CHRM1 primers were created through Primer3 and using National Center for Biotechnology Information (NCBI) blast to confirm specificity to CHRM1 and no other genes.

PRESTO-Tango

We used the National Institute of Mental Health's Psychoactive Drug Screening Program at the University of North Carolina to perform PRESTO-Tango (*37*) analysis of more than 350 nonolfactory GPCRs in the presence or absence of L-DOPA. Top hits from the PRESTO-Tango analysis were manually compared to fragments per kilobase of transcript per million mapped reads (FPKM) from an RNA-seq study of LMC and DMC.

In vivo CRISPR screen

We used lentiviral transduction to deliver dox-inducible Cas9 to WM46 cells and pulled tightly controlled clones and verified by Western blot. The nonolfactory GPCR CRISPR library was transduced with lentivirus with a multiplicity of infection (MOI) of less than 1. A total of 1,000,000 cells were injected subcutaneously in SCID mice. After 7 days of tumor formation, mice were fed dox chow to activate Cas9. After 56 days, tumors were harvested and frozen for sequencing.

Genomic DNA was extracted, and 30 independent PCRs were used to amplify the single-guide RNA (sgRNA) sequences (100 ng of DNA per reaction). Pooled PCR products were prepared for library construction and sequencing via MiSeq (Illumina).

Demultiplexed FASTQ files were processed using cutadapt 1.15. The number of reads for each sgRNA was estimated using the MAGeCK 0.5.7 count module. Reads for each sgRNA were normalized as follows

$$\text{Normalized reads per sgRNA} = \left[\frac{\text{Reads per sgRNA}}{\text{Total number of reads for all sgRNAs in the sample}}\right] \times \text{Average number of reads per sample}$$

If a given sgRNA was not represented in two or more control tumors (i.e., tumors that were not subject to dox selection), we removed the sgRNA from our downstream analysis. Normalized reads for each sgRNA were averaged over each condition (+ dox and – dox), and the fold change (FC) was calculated as

$$\text{FC per sgRNA} = \frac{\text{Average read number per sgRNA in + dox replicates}}{\text{Average read number per sgRNA in – dox replicates}}$$

For dropout hit identification, we chose genes targeted by more than or equal to two sgRNAs that show an FC of at least 0.1. Genes were ranked on the basis of the average FC of all represented sgRNA targeting the gene.

RNA-seq of MCs

RNA was extracted by using an RNeasy kit (Qiagen, Hilden, Germany; catalog no. 74014) following the manufacturer's instructions. All RNA-seq libraries were prepared by using the NEBNext Poly(A) mRNA Magnetic Isolation Module followed by NEBNext Ultra Directional RNA Library Prep Kit for Illumina (both from New England Biolabs, Ipswich, MA). Library quality was analyzed by using Agilent BioAnalyzer 2100 (Agilent, Santa Clara, CA), and libraries were quantified by using NEB Library Quantification Kits (New England Biolabs). Libraries were then sequenced by using a NextSeq500 platform (75 base pairs, single-end reads) (Illumina). All RNA-seq was aligned by using RNA STAR under default settings to *Homo sapiens* UCSC hg19 (RefSeq and Gencode gene annotations). FPKM generation and differential expression analysis were performed by using DESeq2.

Immunohistochemistry and quantification

Formalin-fixed paraffin-embedded (FFPE) human skin tissue sections from organotypic tissue were stained for MITF (NCL-L-MITF, Leica Biosystems, Nussloch, Germany), MelanA (NCL-L-MITF, Leica Biosystems), and Ki67 (NCL-L-Ki67-MM1, Leica Biosystems). Staining was performed following the manufacturer's protocol for high-temperature antigen unmasking technique for paraffin sections. For melanin staining, FFPE tissue was subjected to Fontana-Masson histochemical stain as previously described (*21*, *22*). Tissue section quantification was performed according to previous reports (*22*). Briefly, 10× photomicrograph images of representative tissue sections

were taken using Keyence BZ-X710 (Itasca, IL, USA). Tiff files of the images were saved and transferred to FIJI (ImageJ). Images corresponding to the single specific color were then analyzed to determine the number of pixels in each sample and normalized to epidermal area. The numbers of pixels representing MelanA staining were normalized to the total amount of epidermal area.

DAG sensor

DAG sensor kit was purchased from Montana Molecular (#D0300G Green Down DAG Assay Kit). Using the protocol provided, we transduced human embryonic kidney (HEK) 293T with DAG sensor, CHRM1, and sodium butyrate. Cells were plated in a black-walled 96-well plate with 50,000 cells per well. One hour before reading, cells receiving combination treatment (DOPA and ACh and/or pirenzepine and ACh) were pretreated with either 100 μM DOPA or 200 μM pirenzepine. Drugs were injected in a 25-μl volume into a well volume of 150 μl. The 96-well plate was read using a Cytation 5 plate reader from BioTek using a green filter set (excitation, 485/20; emission, 528/20; extended gain). Reads were conducted every 3 s for up to 5 min.

Measurement of DOPA and dopamine in cells and media

L-DOPA and dopamine were determined by The Metabolomics Core Facility at The Research Institute, Children Hospital of Philadelphia (https://research.chop.edu/metabolomic-core) as follows: The concentration was determined using the Agilent Triple Quad 6410B MS coupled with LC, Agilent 1260 Infinity as described (*1*). Briefly, cells were scraped from tissue culture plates and immediately brought to the core where cells were treated with 4% perchloric acid (PCA) followed by treatment with KOH to neutralize the PCA. Then, 300 μl of cell extract or untreated media was spiked with known amount of dopamine-1,1,2,2-D4-HCL (D4-dopamine), which was used as internal standard for determining the unknown concentration of DOPA or dopamine in cells or media. Then, ethyl alcohol and pyridine (4:1 solution) were added and sample was derivatized with ethyl chloroformate. Then, sample was extracted twice with 2 ml of hexane:ethylacetate (1:1 mixture), evaporated to dryness at room temperature under nitrogen flow, and reconstituted in 100 μl of mixture methanol and formic acid solution (0.1%) in pure H_2O (1:1 mixture). Last, samples were transferred into injection vials and run in LC-MS/MS. Separations were performed on Agilent Poroshell 120 EC-C18 column (3 mm by 100 mm, 2.7 μm). Mobile phase consisted of solution A (0.1% formate in water) and solution B (0.1% formate in acetonitrile with 0.005% trifluoroacetic acid). LC flow was directed into waste for the first 2.5 min and then diverted into MS for the next 4.5 min and back to waste at 7 min. MS/MS conditions were as follows: capillary voltage was 4000 V, nebulizer was set at 25 psi, and drying gas temperature was 350°C. Fragmentor and collision energy voltages were established for each individual compound by MassHunter Optimizer software. Analyte was monitored using multiple reaction monitoring. For measurement of DOPA, we used MRM 442-324; for dopamine, MRM 370-252; and for D4-dopamine, MRM 374-256. The concentrations were determined by the area under the chromatogram of each compound relative to the internal standard.

Melanin assay

Cells (1×10^5) were seeded uniformly on six-well tissue culture plates. Cells were treated with vehicle controls, DOPA, or PTU for 7 days. Cells were then trypsinized and counted, and pellets containing 300,000 cells were spun at 300*g* for 5 min. The cell pellets were solubilized in 120 μl of 1 M NaOH and boiled at 100°C for 5 min. The optical density of the resulting solution was read at 450 nm using an Emax microplate reader (Molecular Devices, Sunnyvale, CA, USA). The absorbance was normalized to a control pellet of 300,000 WM46 cells. All melanin assays were repeated at least three times and each time performed in triplicate.

Statistical analysis

All statistical analysis was performed using GraphPad Prism 8 (GraphPad Software, La Jolla, CA, USA). No statistical methods were used to predetermine sample size. Details of each statistical test used are included in the figure legends.

SUPPLEMENTARY MATERIALS

Supplementary material for this article is available at https://science.org/doi/10.1126/sciadv.abn4007

View/request a protocol for this paper from *Bio-protocol*.

REFERENCES AND NOTES

1. O. Hamid, C. Robert, A. Daud, F. S. Hodi, W. J. Hwu, R. Kefford, J. D. Wolchok, P. Hersey, R. W. Joseph, J. S. Weber, R. Dronca, T. C. Gangadhar, A. Patnaik, H. Zarour, A. M. Joshua, K. Gergich, J. Elassaiss-Schaap, A. Algazi, C. Mateus, P. Boasberg, P. C. Tumeh, B. Chmielowski, S. W. Ebbinghaus, X. N. Li, S. P. Kang, A. Ribas, Safety and tumor responses with lambrolizumab (anti-PD-1) in melanoma. *N. Engl. J. Med.* **369**, 134–144 (2013).
2. A. Ribas, O. Hamid, A. Daud, F. S. Hodi, J. D. Wolchok, R. Kefford, A. M. Joshua, A. Patnaik, W. J. Hwu, J. S. Weber, T. C. Gangadhar, P. Hersey, R. Dronca, R. W. Joseph, H. Zarour, B. Chmielowski, D. P. Lawrence, A. Algazi, N. A. Rizvi, B. Hoffner, C. Mateus, K. Gergich, J. A. Lindia, M. Giannotti, X. N. Li, S. Ebbinghaus, S. P. Kang, C. Robert, Association of pembrolizumab with tumor response and survival among patients with advanced melanoma. *JAMA* **315**, 1600–1609 (2016).
3. Surveillance, Epidemiology, and End Results Program, Cancer stat facts: Melanoma of the skin (2019).
4. I. F. dos S. Videira, D. F. L. Moura, S. Magina, Mechanisms regulating melanogenesis. *An. Bras. Dermatol.* **88**, 76–83 (2013).
5. K. Jimbow, W. C. Quevedo, T. B. Fitzpatrick, G. Szabo, Some aspects of melanin biology: 1950-1975. *J. Invest. Dermatol.* **67**, 72–89 (1976).
6. K. Iozumi, G. E. Hoganson, R. Pennella, M. A. Everett, B. B. Fuller, Role of tyrosinase as the determinant of pigmentation in cultured human melanocytes. *J. Invest. Dermatol.* **100**, 806–811 (1993).
7. K. Wakamatsu, R. Kavanagh, A. L. Kadekaro, S. Terzieva, R. A. Sturm, S. Leachman, Z. Abdel-Malek, S. Ito, Diversity of pigmentation in cultured human melanocytes is due to differences in the type as well as quantity of melanin. *Pigment Cell Res.* **19**, 154–162 (2006).
8. R. A. Sturm, Molecular genetics of human pigmentation diversity. *Hum. Mol. Genet.* **18**, R9–R17 (2009).
9. K. H. Kaidbey, P. P. Agin, R. M. Sayre, A. M. Kligman, Photoprotection by melanin—A comparison of black and Caucasian skin. *J. Am. Acad. Dermatol.* **1**, 249–260 (1979).
10. H. M. Gloster Jr., K. Neal, Skin cancer in skin of color. *J. Am. Acad. Dermatol.* **55**, 741–760 (2006).
11. R. M. Halder, K. M. Bang, Skin cancer in blacks in the United States. *Dermatol. Clin.* **6**, 397–405 (1988).
12. H. M. Yang, S. J. Hsiao, D. F. Schaeffer, C. Lai, H. E. Remotti, D. Horst, M. M. Mansukhani, B. A. Horst, Identification of recurrent mutational events in anorectal melanoma. *Mod. Pathol.* **30**, 286–296 (2017).
13. A. Callahan, W. F. Anderson, S. Patel, J. S. Barnholtz-Sloan, J. S. Bordeaux, M. A. Tucker, M. R. Gerstenblith, Epidemiology of anorectal melanoma in the United States: 1992 to 2011. *Dermatol. Surg.* **42**, 94–99 (2016).
14. E. S. Hong, H. Zeeb, M. H. Repacholi, Albinism in Africa as a public health issue. *BMC Public Health* **6**, 212 (2006).
15. C. J. Witkop, Albinism. *Clin. Dermatol.* **7**, 80–91 (1989).
16. S. K. Kiprono, B. M. Chaula, H. Beltraminelli, Histological review of skin cancers in African Albinos: A 10-year retrospective review. *BMC Cancer* **14**, 157 (2014).
17. J. B. Mabula, P. L. Chalya, M. D. Mchembe, H. Jaka, G. Giiti, P. Rambau, N. Masalu, E. Kamugisha, S. Robert, J. M. Gilyoma, Skin cancers among Albinos at a university teaching hospital in Northwestern Tanzania: A retrospective review of 64 cases. *BMC Dermatol.* **12**, 5 (2012).

18. T. Hirobe, How are proliferation and differentiation of melanocytes regulated? *Pigment Cell Melanoma Res.* **24**, 462–478 (2011).
19. M. Cichorek, M. Wachulska, A. Stasiewicz, A. Tymińska, Skin melanocytes: Biology and development. *Postepy Dermatol. Alergol.* **30**, 30–41 (2013).
20. K. Buac, M. Xu, J. Cronin, A. T. Weeraratna, S. M. Hewitt, W. J. Pavan, NRG1/ERBB3 signaling in melanocyte development and melanoma: Inhibition of differentiation and promotion of proliferation. *Pigment Cell Melanoma Res.* **22**, 773–784 (2009).
21. C. A. Natale, E. K. Duperret, J. Zhang, R. Sadeghi, A. Dahal, K. T. O'Brien, R. Cookson, J. D. Winkler, T. W. Ridky, Sex steroids regulate skin pigmentation through nonclassical membrane-bound receptors. *Elife* **5**, e15104 (2016).
22. C. A. Natale, J. Li, J. Zhang, A. Dahal, T. Dentchev, B. Z. Stanger, T. W. Ridky, Activation of G protein-coupled estrogen receptor signaling inhibits melanoma and improves response to immune checkpoint blockade. *Elife* **7**, e31770 (2018).
23. I. Suzuki, R. D. Cone, S. Im, J. Nordlund, Z. A. Abdel-Malek, Binding of melanotropic hormones to the melanocortin receptor MC1R on human melanocytes stimulates proliferation and melanogenesis. *Endocrinology* **137**, 1627–1633 (1996).
24. P. Valverde, E. Healy, I. Jackson, J. L. Rees, A. J. Thody, Variants of the melanocyte–stimulating hormone receptor gene are associated with red hair and fair skin in humans. *Nat. Genet.* **11**, 328–330 (1995).
25. G. Hunt, S. Kyne, K. Wakamatsu, S. Ito, A. J. Thody, Nle^{4}DPhe^{7}α-melanocyte-stimulating hormone increases the eumelanin:phaeomelanin ratio in cultured human melanocytes. *J. Invest. Dermatol.* **104**, 83–85 (1995).
26. S. A. Burchill, S. Ito, A. J. Thody, Effects of melanocyte-stimulating hormone on tyrosinase expression and melanin synthesis in hair follicular melanocytes of the mouse. *J. Endocrinol.* **137**, 189–195 (1993).
27. J. D'Orazio, D. E. Fisher, Central role for cAMP signaling in pigmentation and UV resistance. *Cell Cycle* **10**, 8–9 (2011).
28. Y. Chudnovsky, A. E. Adams, P. B. Robbins, Q. Lin, P. A. Khavari, Use of human tissue to assess the oncogenic activity of melanoma-associated mutations. *Nat. Genet.* **37**, 745–749 (2005).
29. A. S. McNeal, K. Liu, V. Nakhate, C. A. Natale, E. K. Duperret, B. C. Capell, T. Dentchev, S. L. Berger, M. Herlyn, J. T. Seykora, T. W. Ridky, CDKN2B loss promotes progression from benign melanocytic nevus to melanoma. *Cancer Discov.* **5**, 1072–1085 (2015).
30. V. del Marmol, F. Beermann, Tyrosinase and related proteins in mammalian pigmentation. *FEBS Lett.* **381**, 165–168 (1996).
31. Q. Chen, D. Zhou, Z. Abdel-Malek, F. Zhang, P. S. Goff, E. V. Sviderskaya, K. Wakamatsu, S. Ito, S. S. Gross, J. H. Zippin, Measurement of melanin metabolism in live cells by [U-^{13}C]-L-tyrosine fate tracing using liquid chromatography-mass spectrometry. *J. Invest. Dermatol.* **141**, 1810–1818 (2021).
32. A. Slominski, G. Moellmann, E. Kulinska, L-Tyrosine, L-DOPA, and Tyrosinase as positive regulators of the subcellular apparatus of melanogenesis in bomirski Ab amelanotic melanoma cells. *Pigment Cell Res.* **2**, 109–116 (1989).
33. K. E. Paschkis, A. Cantarow, W. M. Hart, A. E. Rakoff, Inhibitory action of thiouracil, thiocarbamide and other compounds on melanin formation by tyrosinase. *Proc. Soc. Exp. Biol. Med.* **57**, 37–39 (1944).
34. S. H. Dieke, Pigmentation and hair growth in black rats, as modified by the chronic administration of thiourea, phenyl thiourea and alphanaphthyl thiourea. *Endocrinology* **40**, 123–136 (1947).
35. C. D. Marsden, J. D. Parkes, J. E. Rees, A year's comparison of treatment of patients with Parkinson's disease with levodopa combined with carbidopa versus treatment with levodopa alone. *Lancet* **2**, 1459–1462 (1973).
36. V. M. Lopez, C. L. Decatur, W. D. Stamer, R. M. Lynch, B. S. McKay, L-DOPA is an endogenous ligand for OA1. *PLOS Biol.* **6**, E236 (2008).
37. W. K. Kroeze, M. F. Sassano, X. P. Huang, K. Lansu, J. D. McCorvy, P. M. Giguère, N. Sciaky, B. L. Roth, PRESTO-Tango as an open-source resource for interrogation of the druggable human GPCRome. *Nat. Struct. Mol. Biol.* **22**, 362–369 (2015).
38. R. Hammer, C. P. Berrie, N. J. M. Birdsall, A. S. V. Burgen, E. C. Hulme, Pirenzepine distinguishes between different subclasses of muscarinic receptors. *Nature* **283**, 90–92 (1980).
39. A. N. Pronin, Q. Wang, V. Z. Slepak, Teaching an old drug new tricks: Agonism, antagonism, and biased signaling of pilocarpine through M3 muscarinic acetylcholine receptor. *Mol. Pharmacol.* **92**, 601–612 (2017).
40. I. Wessler, C. J. Kirkpatrick, K. Racké, Non-neuronal acetylcholine, a locally acting molecule, widely distributed in biological systems: Expression and function in humans. *Pharmacol. Therapeut.* **77**, 59–79 (1998).
41. H. Kurzen, I. Wessler, C. J. Kirkpatrick, K. Kawashima, S. A. Grando, The non-neuronal cholinergic system of human skin. *Horm. Metab. Res.* **39**, 125–135 (2007).
42. T. Schlereth, F. Birklein, K. An Haack, S. Schiffmann, H. Kilbinger, C. J. Kirkpatrick, I. Wessler, In vivo release of non-neuronal acetylcholine from the human skin as measured by dermal microdialysis: Effect of botulinum toxin. *Br. J. Pharmacol.* **14**, 183–187 (2006).
43. Z. Tang, C. Li, B. Kang, G. Gao, C. Li, Z. Zhang, GEPIA: A web server for cancer and normal gene expression profiling and interactive analyses. *Nucleic Acids Res.* **45**, W98–W102 (2017).
44. P. H. Tewson, S. Martinka, N. C. Shaner, T. E. Hughes, A. M. Quinn, New DAG and cAMP sensors optimized for live-cell assays in automated laboratories. *J. Biomol. Screen.* **21**, 298–305 (2016).
45. Q. Q. Yin, L. H. Xu, M. Zhang, C. Xu, Muscarinic acetylcholine receptor M1 mediates prostate cancer cell migration and invasion through hedgehog signaling. *Asian J. Androl.* **20**, 608–614 (2018).
46. C. Murga, L. Laguinge, R. Wetzker, A. Cuadrado, J. S. Gutkind, Activation of Akt/protein kinase B by G protein-coupled receptors. A role for alpha and beta gamma subunits of heterotrimeric G proteins acting through phosphatidylinositol-3-OH kinasegamma. *J. Biol. Chem.* **273**, 19080–19085 (1998).
47. Z. G. Goldsmith, D. N. Dhanasekaran, G protein regulation of MAPK networks. *Oncogene* **26**, 3122–3142 (2007).
48. H. Davies, G. R. Bignell, C. Cox, P. Stephens, S. Edkins, S. Clegg, J. Teague, H. Woffendin, M. J. Garnett, W. Bottomley, N. Davis, E. Dicks, R. Ewing, Y. Floyd, K. Gray, S. Hall, R. Hawes, J. Hughes, V. Kosmidou, A. Menzies, C. Mould, A. Parker, C. Stevens, S. Watt, S. Hooper, H. Jayatilake, B. A. Gusterson, C. Cooper, J. Shipley, D. Hargrave, K. Pritchard-Jones, N. Maitland, G. Chenevix-Trench, G. J. Riggins, D. D. Bigner, G. Palmieri, A. Cossu, A. Flanagan, A. Nicholson, J. W. C. Ho, S. Y. Leung, S. T. Yuen, B. L. Weber, H. F. Seigler, T. L. Darrow, H. Paterson, R. Wooster, M. R. Stratton, P. A. Futreal, Mutations of the BRAF gene in human cancer. *Nature* **417**, 949–954 (2002).
49. L. A. Fecher, R. K. Amaravadi, K. T. Flaherty, The MAPK pathway in melanoma. *Curr. Opin. Oncol.* **20**, 183–189 (2008).
50. Z. Wang, Y. Li, A. Ahmad, S. Banerjee, A. S. Azmi, D. Kong, C. Wojewoda, L. Miele, F. H. Sarkar, Down-regulation of Notch-1 is associated with Akt and FoxM1 in inducing cell growth inhibition and apoptosis in prostate cancer cells. *J. Cell. Biochem.* **112**, 78–88 (2011).
51. A. Miyashita, S. Fukushima, S. Nakahara, J. Yamashita, A. Tokuzumi, J. Aoi, A. Ichihara, H. Kanemaru, M. Jinnin, H. Ihn, Investigation of FOXM1 as a potential new target for melanoma. *PLOS ONE* **10**, e0144241 (2015).
52. C. Bonet, S. Giuliano, M. Ohanna, K. Bille, M. Allegra, J. P. Lacour, P. Bahadoran, S. Rocchi, R. Ballotti, C. Bertolotto, Aurora B is regulated by the mitogen-activated protein kinase/extracellular signal-regulated kinase (MAPK/ERK) signaling pathway and is a valuable potential target in melanoma cells. *J. Biol. Chem.* **287**, 29887–29898 (2012).
53. X. Wang, H. Kiyokawa, M. B. Dennewitz, R. H. Costa, The Forkhead box m1b transcription factor is essential for hepatocyte DNA replication and mitosis during mouse liver regeneration. *Proc. Natl. Acad. Sci. U.S.A.* **99**, 16881–16886 (2002).
54. D. R. Wonsey, M. T. Follettie, Loss of the forkhead transcription factor FoxM1 causes centrosome amplification and mitotic catastrophe. *Cancer Res.* **65**, 5181–5189 (2005).
55. T. Ito, K. Kohashi, Y. Yamada, A. Maekawa, M. Kuda, M. Furue, Y. Oda, Prognostic significance of forkhead box M1 (FoxM1) expression and antitumour effect of FoxM1 inhibition in melanoma. *Histopathology* **69**, 63–71 (2016).
56. G. B. Liao, X. Z. Li, S. Zeng, C. Liu, S. M. Yang, L. Yang, C. J. Hu, J. Y. Bai, Regulation of the master regulator FOXM1 in cancer. *Cell Commun. Signal.* **16**, 57 (2018).
57. J. H. Bushweller, Targeting transcription factors in cancer—From undruggable to reality. *Nat. Rev. Cancer* **19**, 611–624 (2019).
58. M. V. Gormally, T. S. Dexheimer, G. Marsico, D. A. Sanders, C. Lowe, D. Matak-Vinkoviä, S. Michael, A. Jadhav, G. Rai, D. J. Maloney, A. Simeonov, S. Balasubramanian, Suppression of the FOXM1 transcriptional programme via novel small molecule inhibition. *Nat. Commun.* **5**, 5165 (2014).
59. M. Herlyn, M. L. Mancianti, J. Jambrosic, J. B. Bolen, H. Koprowski, Regulatory factors that determine growth and phenotype of normal human melanocytes. *Exp. Cell Res.* **179**, 322–331 (1988).
60. Y. Ziegler, M. J. Laws, V. Sanabria Guillen, S. H. Kim, P. Dey, B. P. Smith, P. Gong, N. Bindman, Y. Zhao, K. Carlson, M. A. Yasuda, D. Singh, Z. Li, D. El-Ashry, Z. Madak-Erdogan, J. A. Katzenellenbogen, B. S. Katzenellenbogen, Suppression of FOXM1 activities and breast cancer growth in vitro and in vivo by a new class of compounds. *NPJ Breast Cancer* **5**, 45 (2019).
61. I. Wierstra, J. Alves, Cyclin E/Cdk2, P/CAF, and E1A regulate the transactivation of the c-myc promoter by FOXM1. *Biochem. Biophys. Res. Commun.* **368**, 107–115 (2008).
62. H. Pan, Y. Zhu, W. Wei, S. Shao, X. Rui, Transcription factor FoxM1 is the downstream target of c-Myc and contributes to the development of prostate cancer. *World J. Surg. Oncol.* **16**, 59 (2018).
63. D. Mitra, X. Luo, A. Morgan, J. Wang, M. P. Hoang, J. Lo, C. R. Guerrero, J. K. Lennerz, M. C. Mihm, J. A. Wargo, K. C. Robinson, S. P. D. Devi, J. C. Vanover, J. A. D'Orazio, M. McMahon, M. W. Bosenburg, K. M. Haigis, D. A. Haber, Y. Wang, D. E. Fisher, An ultraviolet-radiation-independent pathway to melanoma carcinogenesis in the red hair/fair skin background. *Nature* **491**, 449–453 (2012).

64. S. Alaluf, D. Atkins, K. Barrett, M. Blount, N. Carter, A. Heath, Ethnic variation in melanin content and composition in photoexposed and photoprotected human skin. *Pigment Cell Res.* **15**, 112–118 (2002).
65. A. Slominski, P. Daniel, L-Dopa binding sites in rodent melanoma cells. *Biochim. Biophys. Acta* **1139**, 324–328 (1992).
66. A. Slominski, R. Paus, Towards defining receptors for l-tyrosine and l-DOPA. *Mol. Cell. Endocrinol.* **99**, C7–C11 (1994).
67. A. Slominski, M. A. Zmijewski, J. Pawelek, L-tyrosine and L-dihydroxyphenylalanine as hormone-like regulators of melanocyte functions. *Pigment Cell Melanoma Res.* **25**, 14–27 (2012).
68. A. Slominski, R. Paus, Are L-tyrosine and L-dopa hormone-like bioregulators? *J. Theor. Biol.* **143**, 123–138 (1990).
69. M. M. Wick, L. Byers, E. Frei, L-dopa: Selective toxicity for melanoma cells in vitro. *Science* **197**, 468–469 (1977).
70. M. M. Wick, Levodopa and dopamine analogs as DNA polymerase inhibitors and antitumor agents in human melanoma. *Cancer Res.* **40**, 1414–1418 (1980).
71. M. M. Wick, L-Dopa methyl ester as a new antitumour agent. *Nature* **269**, 512–513 (1977).
72. R. Buchli, A. Ndoye, J. Arredondo, R. J. Webber, S. A. Grando, Identification and characterization of muscarinic acetylcholine receptor subtypes expressed in human skin melanocytes. *Mol. Cell. Biochem.* **228**, 57–72 (2001).
73. W. H. Chua, V. Balakrishnan, Y. H. Chan, L. Tong, Y. Ling, B. L. Quah, D. Tan, Atropine for the treatment of childhood myopia. *Ophthalmology* **113**, 2285–2291 (2006).
74. A. Spinks, J. Wasiak, Scopolamine (hyoscine) for preventing and treating motion sickness. *Cochrane Database Syst. Rev.* **2011**, CD002851 (2011).
75. C. Magnon, S. J. Hall, J. Lin, X. Xue, L. Gerber, S. J. Freedland, P. S. Frenette, Autonomic nerve development contributes to prostate cancer progression. *Science* **341**, 1236361 (2013).
76. L. A. Dalvin, G. M. Damento, B. P. Yawn, B. A. Abbott, J. S. Pulido, Parkinson disease and melanoma: Confirming and reexamining an association. *Mayo Clin. Proc.* **92**, 1070–1079 (2017).
77. J. H. Olsen, S. Friis, K. Frederiksen, J. K. McLaughlin, L. Mellemkjaer, H. Møller, Atypical cancer pattern in patients with Parkinson's disease. *Br. J. Cancer* **92**, 201–205 (2005).
78. J. H. Olsen, S. Friis, K. Frederiksen, Malignant melanoma and other types of cancer preceding parkinson disease. *Epidemiology* **17**, 582–587 (2006).
79. N. Dahodwala, A. Siderowf, M. Xie, E. Noll, M. Stern, D. S. Mandell, Racial differences in the diagnosis of Parkinson's disease. *Mov. Disord.* **24**, 1200–1205 (2009).
80. I. I. Kessler, Epidemiologic studies of Parkinson's disease: II. A hospital-based survey. *Am. J. Epidemiol.* **95**, 308–318 (1972).

Acknowledgments: We thank the University of Pennsylvania Skin Biology and Disease Research–based center for analysis of tissue sections and the Children's Hospital of Philadelphia Metabolomics core for HPLC-MS analysis of DOPA and dopamine in cells and media. GPCR functional data were provided by the National Institute of Mental Health's Psychoactive Drug Screening Program, contract no. HHSN-271-2018-00023-C (NIMH PDSP). The NIMH PDSP is directed by B. L. Roth at the University of North Carolina at Chapel Hill and project officer J. Driscoll at NIMH, Bethesda, MD, USA. **Funding:** T.W.R. is supported by a grant from the NIH/NCI (R01 CA163566, R41CA228695, and R56AR079409) and the Department of Defense (81XWH2110860). This work was also supported in part by the Penn Skin Biology and Diseases Resource–based Center (P30-AR069589). B.S.K. and J.A.K. are supported by grants from the Breast Cancer Research Foundation (BCRF-083 and BCRF-084). M.D. is supported by a grant from the NIH/NCI (F31 CA250316) and by the University of Pennsylvania Dermatology Training Grant (T32AR007465). **Author contributions:** M.D. designed and conducted experiments, performed data collection and analysis, conceptualized and supervised the project, and wrote and reviewed the manuscript. C.A.N. designed and conducted experiments and conceptualized and reviewed the manuscript. I.Y.L. and R.B. conducted experiments and reviewed the manuscript. S.V. performed data analysis. S.H.K., Y.W., and C.R.V. provided methodology and synthesized resources. J.A.K. and B.S.K. provided methodology and resources and reviewed the manuscript. B.C.C. provided resources, performed data analysis, and reviewed the manuscript. M.E.F. conceptualized experiments, provided resources, performed data analysis, and reviewed the manuscript. T.W.R. conceptualized and supervised the project and reviewed the manuscript. **Competing interests:** S.H.K., J.A.K., and B.S.K. are inventors on a PCT patent application (PCT/US2019/026633) covering this technology that was filed by the Board of Trustees of the University of Illinois on 9 April 2019 and was published on 17 October 2019 (WO2019199863A1) and is pending. This patent application was also filed on the same date in Europe, Japan, United States, Canada, China, and Australia; these applications have all been published and are pending. The other authors declare no competing interests. **Data and materials availability:** All data needed to evaluate the conclusions in the paper are present in the paper and/or the Supplementary Materials. The NB-class FOXM1 inhibitor compounds can be provided by J.A.K. and B.S.K. pending scientific review and a completed material transfer agreement. Requests for the compounds should be submitted to: jkatzene@illinois.edu and katzenel@illinois.edu.

Submitted 23 November 2021
Accepted 14 July 2022
Published 2 September 2022
10.1126/sciadv.abn4007

ScienceAdvances

Endogenous DOPA inhibits melanoma through suppression of CHRM1 signaling

Miriam DoepnerInyoung LeeChristopher A. NataleRoderick BrathwaiteSwati VenkatSung Hoon KimYiliang WeiChristopher R. VakocBrian C. CapellJohn A. KatzenellenbogenBenita S. KatzenellenbogenMichael E. FeiginTodd W. Ridky

Sci. Adv., 8 (35), eabn4007. • DOI: 10.1126/sciadv.abn4007

Science Advances (ISSN) is published by the American Association for the Advancement of Science. 1200 New York Avenue NW, Washington, DC 20005. The title *Science Advances* is a registered trademark of AAAS.